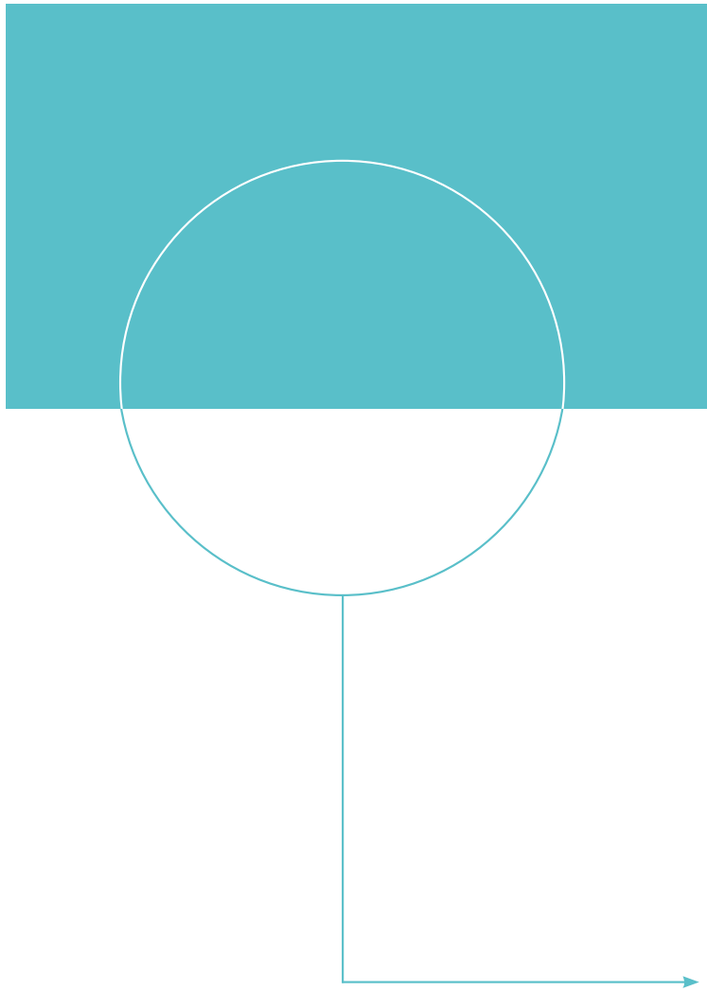

Master's thesis

2019

Saber Samee

NTNU
Norwegian University of
Science and Technology
Faculty of Engineering
Department of Energy and Process Engineering

Saber Samee

Multiphysics simulation of physical processes with different time constants

June 2019

NTNU
Norwegian University of
Science and Technology

NTNU
Norwegian University of
Science and Technology

NTNU

Norwegian University of
Science and Technology

Multiphysics simulation of physical processes with different time constants

Saber Samee

Mechanical Engineering
Submission date: June 2019
Supervisor: Ivar S. Ertesvåg
Co-supervisor: Dr.Geir Berge

Norwegian University of Science and Technology
Department of Energy and Process Engineering

Preface

This master's thesis is the conclusion of a five-year integrated master's programme in mechanical engineering at NTNU (2014-2019), Trondheim. The work is part of the engagements of the Department of Energy Process Engineering at NTNU and Petrell AS within multiphysics. The work on completing the thesis introduced me to the realm of multiphysics simulation and made me appreciate the complexity of the field. Realizing the potential of multirate approach to remarkably reduce the simulation time, without significantly compromising accuracy, fueled the motivation for this thesis work. Also, the analytical work on the well-reservoir dynamics proved to be a very challenging yet rewarding experience. The thesis work was a valuable lesson to the process of scientific publication in addition to the field of researching and acquiring knowledge independently.

I am grateful to my supervisor Professor Ivar Ståle Ertesvåg for following up the work throughout the thesis and for being available for guidance when needed. I also want to thank my colleagues at Petrell AS, especially Tore Flåtten and Torgeir Ustad, whom would engage in fruitful discussions with me about relevant topics in this thesis. I feel privileged for having had Dr.Geir Berge at Petrell AS as my co-supervisor and mentor during this work. His continuous assistance and deep knowledge in the field helped paving the way to the end results. Last, my kindest thanks to my family and friends for their support and encouragement throughout my years of study.

Saber Samee
Trondheim, June 2019

Problem Description

Multiphysics is about the mutual influences of different physical phenomena and their dynamic interactions. It is worth noting that it is in dynamic systems, the mutual effects are important. Transient problems are simulated in time with time steps that are adapted to the time gradient of the specific case. Multiphysics problems can in many instances involve different physical phenomena with different time gradients and, hence, require time steps of different lengths. When the differences in time gradients are large, physics with small time gradients can experience physics with large gradients as an almost constant boundary condition. Small gradient problems can adapt fast to the boundary conditions. In view of this, it is tempting to investigate the subject with the perspective of reducing simulation time and still maintain an acceptable accuracy.

Abstract

Reservoir simulations can be costly and time-consuming as a typical reservoir can be in the size-range of hundreds of millions of cubic meters and producing for decades. In an attempt to reduce the simulation time while maintaining an acceptable accuracy, a multi-rate approach is proposed in this study. The approach is based on dividing the system into a fast and a slow subsystem. The ratio between the velocities in the well and the reservoir was shown to be around 10^4 in the simulations. Therefore, the well and the reservoir are classified as the fast and the slow subsystem, respectively. Reservoir permeability and well length are used as variables to asses the effects of this approach in regard to accuracy.

The idea is that a fast subsystem adapts to changes much more rapidly than a slow subsystem, hence the values of each variable in the fast subsystem can be assumed to be constant for short periods of time. This is done by deactivating the well subsystem in this study. As a consequence, the system can be simulated with large time steps adapted to the slow subsystem. An another advantage of using multirate approach is that stability issues related to the fast subsystem can be avoided. The time step ratio between the two subsystems was shown to be at least 20 for the cases tested here. The activation and deactivation of the well subsystem is based on pressure difference and a time-period defined by the user. Results from the simulations using the software Brilliant have shown that the simulation time can be reduced by 67% while only deviating by 0.6%. The deviation is measured in regard to the case when the well subsystem is never deactivated.

Sammendrag

Reservoarsimuleringer kan være kostbare og tidkrevende da et typisk reservoar kan være i størrelsesorden av hundrevis av millioner kubikkmeter og produsere i flere tiår. I et forsøk på å redusere simuleringstiden samtidig som å opprettholde akseptabel nøyaktighet, foreslås det en multirate tilnærming i dette studiet. Tilnærmingen er basert på å dele systemet i et raskt og et tregt delsystem. Forholdet mellom strømningshastighetene i brønnen og reservoaret ble vist til å være rundt 10^4. Derfor er brønnen og reservoaret klassifisert som henholdsvis det raske og det trege delsystemet. Reservoarpermeabilitet og brønnlengde er brukt som variabler for å vurdere påvirkningen av denne tilnærmingen i forhold til nøyaktighet.

Tanken er at et raskt delsystem tilpasser seg forandringer mye raskere enn et tregt delsystem. Derfor kan variabelverdiene i det raske delsystemet antas å være konstant i korte perioder. I praksis gjøres det ved å deaktivere brønndelsystemet i dette studiet. Det betyr altså at systemet kan simuleres med store tidssteg tilpasset det trege delsystemet. En annen fordel med denne tilnærmingen er at stabilitetsproblemer i det raske delsystemet kan unngås. Forholdet mellom tidsstegene i de to delsystemene ble vist til å være minst 20 i de tilfellene som ble testet her. Aktivering og deaktivering av brønndelsystem er basert på trykkforskjell og tidsperiode definert av brukeren. Resultater fra simuleringene utført ved hjelp av programvaren Brilliant har vist at ved å godta et avvik på 0.6%, kan simuleringstiden reduseres med 67%. Avviket måles i forhold til en simulering der brønndelsystemet aldri blir deaktivert.

Contents

Preface i

Problem Description ii

Abstract iii

Sammendrag iv

Table of Contents v

Nomenclature viii

1 Introduction 1

1.1 Multiphysics Simulation Using Multirate Approach 1

1.2 Scope 3

1.3 Objective 4

1.4 Outline of Thesis 4

1.5 Motivation 5

2 Coupled Multirate Problems 8

2.1 Multirate Philosophies 8

2.2 Types of Coupled Problems 9

2.3 Coupling Strategies 11

2.3.1 Fast-First Vs. Slow-First 13

2.3.2 Predictor-Corrector 15

2.3.3 Step-Skipping 16

3 Determining Time Constants in a Multiphysics Problem 17

3.1 Time Constant in Multirate Approach 17

3.2 Splitting Parts 18

3.3 Fourier Transform 20

3.4 Eigenvalue Analysis 21

3.5 Order of Magnitude . . . 24
3.6 Self-Adjusting Methods . . . 26
3.7 The Main Six Characteristics of Multirate Approach . . . 26

4 Governing Equations of Well-Reservoir Dynamics 28
4.1 General Assumptions . . . 28
4.2 Reservoir . . . 29
4.2.1 Darcy's Law . . . 29
4.2.2 Pressure and Mass Conservation . . . 30
4.2.3 Energy . . . 31
4.2.4 Transport of Species . . . 32
4.3 Well Flow . . . 33

5 Overview of Physics and Numerical Approaches in a Reservoir 35
5.1 Reservoir Pressure and Temperature . . . 35
5.2 Qualitative Analysis of Well-Reservoir Dynamics . . . 38
5.2.1 General Overview . . . 38
5.2.2 Coupling between the Subsystems . . . 39
5.3 Numerical Approaches to Reservoir Simulation . . . 41
5.3.1 Introduction . . . 41
5.3.2 Review of Numerical Approaches and Approximation Models . . . 41

6 Reservoir Simulation 43
6.1 System Characteristics . . . 43
6.1.1 Multirate Approach in Reservoir Simulation . . . 44
6.1.2 Calculation Sequence in Brilliant . . . 45
6.2 Geometry, Setup and Preliminary Analysis . . . 46
6.3 Verification and Validation . . . 48
6.3.1 Pressure . . . 48
6.3.2 Velocity . . . 49
6.3.3 Intermediate Conclusion . . . 50
6.4 Error Estimation . . . 50
6.5 Time Based Deactivation . . . 51
6.5.1 Results of Varying Length and Permeability . . . 53
6.5.2 Sampling in Reservoir . . . 58
6.6 Pressure Based Deactivation . . . 60

7 Discussion **65**
7.1 Time Consumption Vs. Error 65
7.2 Further Work 68
7.2.1 Hybrid Approach 68
7.2.2 Slow-First Approach With a Jump 69

8 Conclusions **71**
8.1 Conclusions 71

Bibliography **73**

Appendix A Oil and Gas **79**
A.1 Origin of Oil and Gas 79
A.2 Seismic Survey 79
A.3 Reservoir Thermal Properties 81
A.4 Production Enhancement by Injection 82

Appendix B Numerical Stability of Multirate Approach **84**

Appendix C Upscaling of Grid in Reservoir Simulation **86**

Nomenclature

Δh	Difference in height between two points [m]
$\dot{m}''$	Mass flux of a solute in a solution $[\frac{\mathrm{kg}}{\mathrm{m}^2}]$
κ	Intrinsic permeability of porous medium $[\mathrm{m}^2]$
μ	Dynamic viscosity [Pa s]
∇p	Pressure gradient vector $[\frac{\mathrm{Pa}}{\mathrm{m}}]$
ω	Frequency [Hz]
ψ	Total volume porosity $[-]$
ρ	Density of fluid $[\frac{\mathrm{kg}}{\mathrm{m}^3}]$
σ_{ij}	Stress tensor $[\frac{\mathrm{N}}{\mathrm{m}^2}]$
τ	Time representing slow subsystem [s]
τ_c	Time constant of a process [s]
Θ	Temperature [K]
A_s	Cross sectional area of flow in soil or other porous media $[\mathrm{m}^2]$
C	Courant number $[-]$
c	Speed of sound $[\frac{\mathrm{m}}{\mathrm{s}}]$
C_p	Specific heat capacity of fluid at constant pressure $[\frac{\mathrm{J}}{\mathrm{kg\,K}}]$
D	Diffusion coefficient $[\frac{\mathrm{m}^2}{\mathrm{s}}]$
D_p	Particle diameter in a porous medium [m]
h_e	Specific enthalpy $[\frac{\mathrm{J}}{\mathrm{kg}}]$
L	Characteristic length or well length [m]

Pr	Prandtl number [−]
q	Velocity of fluid in porous media $[\frac{\mathrm{m}}{\mathrm{s}}]$
R_c	Parameter referring to the ratio of the time constant in slow subsystem to its corresponding value in the fast subsystem [−]
Re	Reynolds number [−]
Sc	Schmidt number [−]
T	Time representing fast subsystem [s]
t	Time [s]
u	Velocity of fluid $[\frac{\mathrm{m}}{\mathrm{s}}]$
Y_k	Mass fraction of species k [−]

Chapter 1

Introduction

1.1 Multiphysics Simulation Using Multirate Approach

From a simple falling ball through the air to a huge powerful storm, the interactions between the governing laws in each case are often referred to as multiphysics. According to Zhen Liu, a multiphysics problem is defined as "the coupled processes or systems involving more than one simultaneously occurring physical fields and the studies of and knowledge about these processes and systems [1]."

In the early 1940's, when the first digital computers were developed, the common approach to solving multiphysics problems was to split a problem into many smaller problems, and then simulate each at a time. The reason for this is simply due to the scarce computing resources at the time. However, as the computational cost is drastically reduced nowadays, simulating the entire multiphysical system simultaneously is more feasible now than ever. Fig. 1.1 illustrates an example of a multiphysical system.

There are in general different processes involved in a multiphysics problem where each process, or variable, can have its own time constant different than the others. In other words, some variables experience changes much more rapidly than others. One of the researchers who has studied this field from a mathematical point of view is professor Christian Kuehn. In 2015, he published a book by the name of "Multiple Time Scale Dynamics" where he discusses methods to approach such type of problems. One important approach, which forms the basis of the analysis in this thesis work, is splitting the variables into a fast and a slow subsystem depending on their time constant.

Figure 1.1: An example of a multiphysical system that can be simulated numerically[2].

In a conventional multiphysics simulation the entire system is simulated using a single time step which is often dictated by the accuracy or stability limit of the fastest subsystem. This type of approach is often referred to as the single-rate approach[3]. On the contrary, in a multirate time integration approach, or simply multirate approach, different time steps are used in each process, or subsystem, in order to increase the overall efficiency by reducing the number of communication points between the subsystems[4]. However, information between the subsystems need to be exchanged at certain points along a simulation in order to ensure overall accuracy. Multirate approach is a numerical technique for solving a set of equations that describe processes that respond to changes on a widely different time scales[5]. The approach utilizes the different time scales of the components within the system by using different time steps accordingly. Typically, slowly varying components are designated larger time steps than the rapidly varying components. Although the multirate approach is not significantly different from the single-rate approach conceptually, there are still many open questions regarding its theory, implementation and scope of use[6]. It is worth mentioning that the foundation of this thesis work is inspired by seepage of groundwater into a riverbed, which was the topic of the pre-master's project[7].

Reservoir performance simulation, or reservoir simulation in short, is a field where the use of multirate approach can have a huge impact on its associated cost and time consumption. The reason for this is that the flow in the reservoir is much slower than in the well. This motivates splitting of the well and the reservoir into two different subsystems. A typical reservoir can be in the size-range of hundreds of millions of cubic meters and

producing for decades. As a consequence, the overall simulation time can be remarkably reduced. The aim of this thesis work is to look at the possibilities of reducing reservoir simulation time while maintaining an acceptable accuracy. To achieve this, a type of multirate approach is proposed which relies on activating and deactivating, or controlling, the well subsystem for short periods of time. Controlling the well subsystem, on the other hand, is based on either the pressure difference in the system or by a time-period defined by the user. These two specific deactivation approaches are chosen due their compatibility with the simulation software used in this study, which is developed by Petrell AS and is called Brilliant. Matlab is also used to present plots where needed.

The multirate approach has gained a lot of attention recently due to its ability to provide efficient simulations without significant compromise on accuracy. In chemical engineering, for instance, different chemical processes take place on a wide range of time scales rendering single-rate simulation uneconomical[3]. The approach is prominent in the field of power electronics as well. A power electronic system is inherently multirate in which currents and voltages varying differently both in space and time. This in addition to the subcircuits in the system also having different transient rates[8]. Furthermore, in atmospheric models based on nonhydrostatic dynamics, time scales range significantly from microseconds to weeks or more. The major different time scales can be divided into three speed regimes represented by sound speed, internal wave speed, and convective wind velocity[9]. Using multirate approach opens new opportunities now than ever before considering the growing understanding of the field combined with the exponentially growing computational power at disposable.

1.2 Scope

In this study, the relative error of using multirate approach in regard to reservoir simulation is compared with the single-rate approach and not to real world measurements. The reason for this is that reservoir simulations are based on seismic data that are not accurate in the first place[10]. Since it is difficult to separate the error originated from the seismic data from the numerical error, comparing single-rate approach against real worlds measurements is difficult to accomplish with today's technology. In addition, the type of multirate approach used to simulate the cases in this study is tailored to the dynamics of a well-reservoir system. Hence, the results must not be extended to other types of systems without further revision.

1.3 Objective

This thesis work is initiated by Petrell AS with an objective to investigate the possibilities of reducing reservoir simulation time while maintaining an acceptable accuracy using a multirate approach. Hence, an overview of multirate approach and well-reservoir dynamics is to be acquired and understood for the analysis in this study. The multirate approach is a wide concept that comes in different forms and combinations. Therefore, a basic collection of concepts and ideas related to multirate approach is first presented in Chapters 2 and 3, which serve as an introduction to the multirate field. These two chapters are meant to help the user choose the combination that is most suitable for the problem in hand. Last, knowledge from the field of multirate and well-reservoir dynamics is used as a foundation for performing and analysing the reservoir simulations presented in this study.

1.4 Outline of Thesis

The content of this thesis work is structured and presented in the following order:

Chapter 2 presents the literature review on the topic of multirate approach. The chapter introduces the methods of coupling subsystems with each other along with the advantages and disadvantages of each method. A brief comment on stability and convergence aspects of numerical simulations is given in the end of the chapter.

Chapter 3 covers methods that can be used to identify the time constant of each subsystem in a multiphysics problem. The use of the methods are illustrated through quantitative examples. Such type of methods can be useful when trying to determine which subsystem is the fast and which one is the slow. An overview of the six categories of multirate approach is presented in the end of this chapter.

Chapter 4 provides the governing equations that are used in reservoir simulations. The equation system is split into two different parts each representing the flow in the well and the reservoir. The limitations and regions of use of these equations are mentioned this chapter.

Chapter 5 gives an introduction to the well-reservoir dynamics. The chapter also touches on the numerical approaches that are used in the industry in regard to reservoir simula-

tions.

Chapter 6 is devoted to reservoir simulations using Brilliant. Two approaches, building on multirate reasoning, are used to control the well subsystem. The approaches are based on pressure difference and a time-period defined by the user. The results from both approaches are presented and discussed in this chapter.

Chapter 7 covers the discussion on which approach to use to control the well subsystem based on simulation time and error introduced by each approach. Recommendation on further work is given in the end of this chapter.

Chapter 8.1 draws a conclusion based on the results and the discussions in this study.

1.5 Motivation

In this section, a first order ordinary differential equation (ODE) is analysed to better understand why a system of processes with different time scales must be separated numerically. The analysis is based on fast-slow system dynamics. Most of the knowledge in this section is extracted from Kuehn's book[11].

Consider the general ODE initial value problem

$$\frac{dz}{dt} = z' = F(z) \quad , \quad (T_0) = z_0. \tag{1.1}$$

The simplest method that can be used to solve Eq.(1.1) numerically is by using the explicit form of Euler method. A time step h is used such that

$$t_n = T_0 + nh \quad , \quad n = 0, 1, 2, ...,$$

where T_0 is the initial time and n is the number of steps. The ODE can now be descritized as following

$$\frac{z^{n+1} - z^n}{h} = F(z),$$

$$z^{n+1} = z^n + hF(z). \tag{1.2}$$

Eq.(1.2) approximates the value of z in the next time step $n + 1$ using the derivative of z at the current time n. Now consider a system of ODEs where the variables x and y represent the fast and the slow subsystem, respectively.

$$\frac{dx}{dt} = \dot{x} = -\frac{x}{\epsilon},$$

$$\frac{dy}{dt} = \dot{y} = -y.$$

The ϵ here represents the ratio between the time scales of the slow and fast subsystems and is much less than one, i.e. $\epsilon << 1$. The analytical solution of the ODE system is obtained by multiplying by dt and integrating on both sides

$$x(t) = x(0)e^{-t/\epsilon},$$

$$y(t) = y(0)e^{-t}. \tag{1.3}$$

The analytical solution of the ODE system (1.3) shows that the system will decay to zero after a while. However, when using the explicit Euler method as shown earlier, the method experiences instability and the solution diverges as a result. This is illustrated in Fig. 1.2

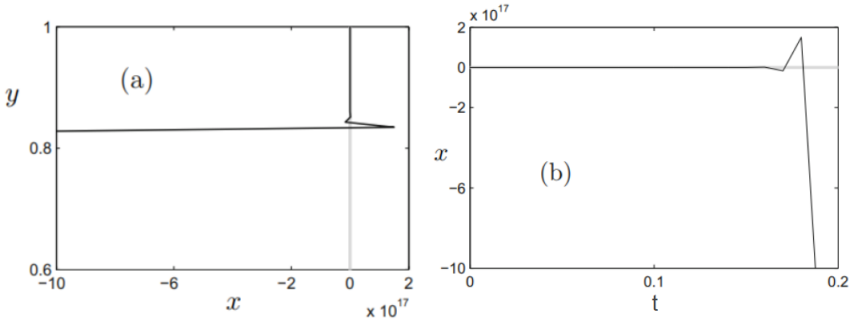

Figure 1.2: Numerical solution of the ODE system using explicit Euler method for $\epsilon = 0.001$ and $h = 0.01$. The grey color shows the analytical solution. Note the large scale for the x-coordinate in the phase space plot (a) and the time series plot (b) [11].

To find out the reason behind this numerical instability, denote the ODE system by $z' = Az$, where $z = (x, y)$ representing the variables in the linear system. Hence, matrix A is given by

$$A = \begin{bmatrix} -\frac{1}{\epsilon} & 0 \\ 0 & -1 \end{bmatrix}.$$

By applying the same procedure that lead to Eq.(1.2), the linear system of ODE equations can now be written as

$$z^{n+1} = z^n + hAz^n = (Id + hA)z^n, \tag{1.4}$$

where I is the identity matrix. Eq.(1.4) can further be written as

$$z^n = (Id + hA)^n z^0 = \begin{bmatrix} (1 - \frac{h}{\epsilon})^n & 0 \\ 0 & (1-h)^n \end{bmatrix} z^0. \tag{1.5}$$

Now consider $(Id + hA)$ from Eq.(1.5) to be equal to k, and let $f = \frac{1}{k} - 1$ such that $k = \frac{1}{1+f}$. By introducing the power n on both sides and taking the lim to infinity

$$\lim_{x\to\infty} k^n = \lim_{x\to\infty} \frac{1}{(1+f)^n} \tag{1.6}$$

Eq.(1.6) shows that if $|k| < 1$, i.e. when $f < -2$ or $f > 0$, k^n converges to zero for $n \to \infty$. This entails that both $(1-h/\epsilon)$ and $(1-h)$ should also have an absolute value less than 1. The latter is easily satisfied as long as the time step h is less than 2. However, the problem arises for the fast component x, where h must satisfy the $0 < h/\epsilon < 2$ condition. Thus, the step size h must be extremely small if the time scale ratio between the subsystems ϵ is very large. Choosing a small time step is undesirable as the total simulation time can be reduced significantly. Therefore, it is preferable to split the system into one fast and one slow subsystem each with a different time step. In other words, a multirate approach must be used to avoid the time step constraint of the fastest subsystem. Typically, the time steps are chosen based on the accuracy and stability constraints of the particular subsystem to optimize the numerical simulation.

Chapter 2

Coupled Multirate Problems

The subsystems in a multirate approach use different time steps for optimal efficiency as mentioned earlier. However, they must be coupled with each other at certain points throughout the simulation in order to exchange information. The rate of communication between the subsystems relies on the grade of their dependency on each other. According to Bernd Markert, a coupled system is "a system of equations which consists of two or more of such interconnected subsystems involving dependent variables that cannot be eliminated on equation level, where an independent solution of any subsystem is impossible without simultaneous solution of the other[12]". This chapter discusses the different types of coupling methods and the advantages and disadvantages corresponding to each method. An overview of this chapter along with chapter 3 is given in Table 3.1 as the content of the two chapters are correlated.

2.1 Multirate Philosophies

Using a multirate approach raises many questions regarding the type and frequency of the communication between each subsystem. There are different philosophies on how subsystems should communicate or be related to each other. The following is an outline of four of these philosophies[12]:

- Monolithic or direct approach: The subsystems are advanced simultaneously in time by the same time step. The time step in this case is restricted by the fastest subsystem, and in order to avoid very small time steps, implicit methods are preferred in such case. If the problem in hand is single-physical (not multiphysical), this approach becomes the same as the traditional single-rate approach.

- Partitioned or iterative approach: The subsystems in this approach are treated as

isolated entities and are advanced with time steps that are most efficient for each one. Each subsystem can be integrated in time by different methods, hence, the time step designated for each subsystem must obey the corresponding accuracy and stability criteria of the method used. Such approach is therefore suitable when the coupling is geometrical. Interaction between the subsystems is viewed as forcing effects that are communicated in between using prediction, substitution and synchronization techniques.

- Fractional-step method: This method involves choosing a suitable numerical sub-algorithms to discretize each subsystem at each time step independently. Thereafter, the sub-algorithms are merged by utilizing a higher-order product method to obtain the time-stepping algorithm for the entire problem at each time step[13].

- Field variable Elimination: This approach depends on eliminating one or more field variables by techniques such as reduction or integral transforms. After doing so the entire system is advanced using a monolithic approach.

The monolithic approach is most suitable when the coupling between the subsystems are highly nonlinear and is best solved simultaneously. Examples of such coupling is conjugate heat transfer with fluid flow[12]. The partitioned approach, on the other hand, is used when the coupling is not profoundly nonlinear while a higher degree of efficiency and accuracy is needed. Fractional step method, in contrast to partitioning method that is based on a field by field decomposition, follows a strategy of time discretization within the time step interval of a field[12]. Moreover, the field variable elimination approach is one of the oldest approaches and is mainly used to special linear problems, which in turn renders the method obsolete in comparison to the other methods mentioned here[12].

2.2 Types of Coupled Problems

In some coupled multiphysics problems such as in fluid-structure interaction, the spatial discretization used in the structure and the fluid subdomain are different from each other. Furtheremore, the dependent variables such as fluid pressure and solid displacement in each subsystem interact at the interface of the two subdomains, hence, such type of coupling between the subsystems is referred to as geometric coupling. In other words, the interaction between the subsystems in a geometric coupling occurs due to boundary conditions or as a result of interface equations[12]. Such type of coupling can be utilized by loosening the coupling in space and solving each subsystem individually. More examples of geometric coupling can also be found in systems such as ocean-atmosphere dynamics in geophysics and core-edge coupling in tokamaks[14]. On the other hand, there are other

types of systems where the subsystems interact with each other within the same spatial domain such as thermal-structure interaction. Heat flux from a thermal source influence the structure at each point throughout the body as heat is a part of the equations that govern the physics of the structure. Hence, this type of coupling, in contrast to the geometric coupling that acts only at the boundary, is referred to as volumetric coupling[12]. Other typical examples of volumetric coupling include electricity and magnetism with hydrodynamics in plasma physics (magnetohydrodynamics), radiation with hydrodynamics in astrophysics and chemical reaction with transport in combustion or subsurface flows (reactive transport)[14].

The coupling strength between the subsystems in both the geometric and volumetric coupling can further be categorized into two types, a strong and a weak coupling. A weak coupling is defined as a one way coupling where a subsystem A can influence subsystem B, but not vice versa[12]. An example of such coupling is the volumetric coupling between a thermal field and a structure such as burning a piece of paper with a lighter for instance. The structure in the paper is severely altered by the heat flux from the flame without affecting the flame itself. On the other hand, strongly coupled subsystems are inherently independent on each other leading to a multiple way interaction and must therefore be updated simultaneously[12]. An example of such system is the geometrical coupling in a fluid-structure system such as in the case of unsteady blood flow in arteries. Due to plaque deposits, the flow of blood in arteries can be severely decreased while the pressure increased as a result[15]. Fig. 2.1 shows that the pressure is higher ahead of the plaque deposits since the velocity of blood flow increases as the channel becomes narrower, which in turn leads to the expansion of the artery. It can be seen from Fig. 2.2 that the maximum pressure and velocity occur at almost the same time, this shows that both elasticity in the artery wall and the blood flow influence each other, hence they are strongly coupled.

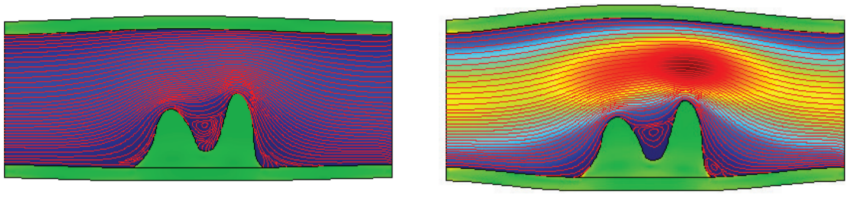

Figure 2.1: Streamlines of spatial velocity field at t=0.1 sec (left) and t=0.215 sec (right). The highest velocity is found in the red region[15].

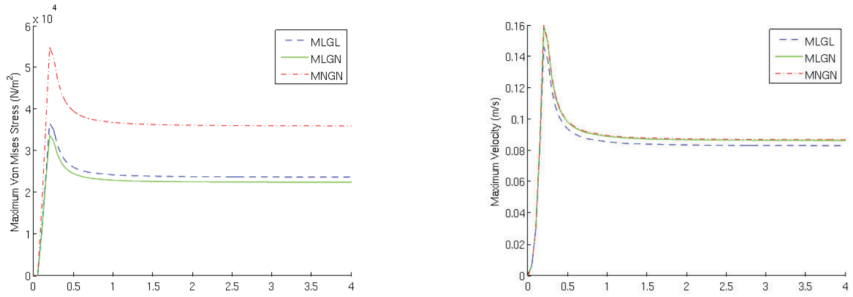

Figure 2.2: The horisontal axis represents time in seconds. Left: Maximum Von Mises stress experienced by the surface of the artery. Right: Maximum velocity profiles. The three models used, MLGL, MLGN and MNGN are not of interest here[15].

The mutual interaction of components in a system can be nonlinear and act on different time scales. Solving such problems require additional theoretical models to account for the coupling mechanisms and describe the behaviour in the system accurately. There are in general three definitions of coupled problems according to Park and Felippa[[16],[17]]:

- Coupled problem: In a coupled problem, the different subsystems interact with each other dynamically. The interaction is mutual and therefore the solution has to take into account the simultaneous analysis of the coupled equations. Obviously, such kind of coupling is associated with strong coupling.
- Coupled multi-field problem: A coupled multi-field problem is characterized by a physical system that is described with different field equations in which the variables in each field can be a function of the other. Every coupled problem is by definition a multi-field problem. An example of such problem is acoustic-structure interaction with the two-field problem coupling the change in structure's displacement with the acoustic pressure field[12].
- Coupled multi-physics problem: A coupled multi-physics problem is described as a problem where multiple physical models are simulated simultaneously. This can be a coupling between two different type of discretization techniques used for each subsystem, or, a coupling between subsystems that represent different phenomena while mutually interacting with each other. A typical example of such system is reaction-diffusion systems where the local chemical reaction is coupled with the diffusive spatial transport[12].

2.3 Coupling Strategies

An effective communication between the subsystems in a multiphysics simulation is essential when it comes to reducing the overall simulation time and achieving accurate results.

Different types of coupling strategies are discussed in more detail in this section.

Whether the overall system is coupled in the bulk (volumetric) or over an interface (geometric), the variables in the subsystems still need to exchange data in a predefined strategy. The coupling strategies, in general, belong into two main coupling classes as following:

- Fully-dynamic coupling: Requires iterations between variables until a certain convergence criteria is met[18]. This strategy is associated with strong coupling.
- Loose coupling: Each subsystem is solved individually while keeping the others fixed[19]. The value of each variable from the other subsystems can for instance be predicted based on previous time steps. This strategy is associated with weak coupling.

In other words, a coupling strategy based on the fully-dynamic coupling yields more accurate results than if based on the loose coupling. However, the latter tends to be faster as there is less communication between the subsystems. If the time scale of two subsystems are close to\overlap each other such as in Fig. 2.3, then these two subsystems become strongly dependent on each other (strongly coupled). Therefore, a fully-dynamic coupling must be used in order to capture the interaction[20]. This can also be seen in the example in Fig. 2.2, where the Von Mises stress in the artery wall and the blood velocity reach their highest at almost the same time. Both profiles follow the same pattern indicating strong dependency between the two properties. On the contrary, if the difference between the time scale of the two subsystems are significant, then their interaction becomes negligible, and thus, the loose coupling should be used for efficiency[20]. Consequently, the definition of strong and weak coupling, i.e. multiple ways and one way coupling, respectively, is now expanded to include the time scale of the subsystems. Choosing a coupling strategy based on the loose coupling class entails solving for either the fast or the slow subsytem first, and then exhange data with the other subsystem (in case of having only two subsystems).

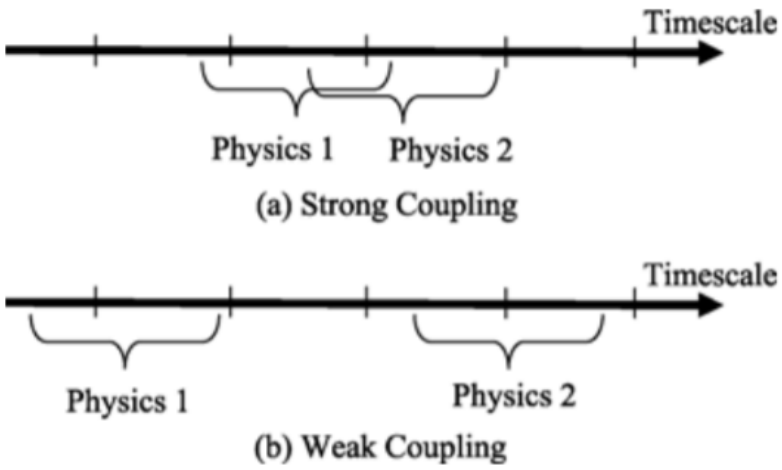

Figure 2.3: Coupling between two physics\subsystems[20].

After having determined a class of coupling based on the time scale and coupling strength between the subsystems in a multiphysics problem, the next step is to choose a suitable coupling strategy. The following three subsections present different coupling strategies that enables exchange of data between the subsystems.

2.3.1 Fast-First Vs. Slow-First

Numerical stability criteria imposes restrictions on the time step siz in a simulation when using an explicit time discretization method. This can for instance be due to restrictions tied to the CFL-condition[21] related to the advection parts. Hence, the time step used in the slowest subsystem can be much larger than the corresponding time step in faster subsystems. However, it should be noticed that it might be necessary to choose small time step even when using implicit methods[22]. This is to ensure convergence when many equations are solved iteratively within a subsystem. Figs. 2.4 and 2.5 show examples of coupling strategies where either the fast or the slow subsystem is solved first (loose coupling). The macro time step Δt and the micro time step Δt_s in this subsection refer to the time steps in the slow and the fast subsystem, respectively. In the rest of this study, the time step in the slow subsystem is referred to as ΔT, while in the fast subsystem, $\Delta \tau$ is used.

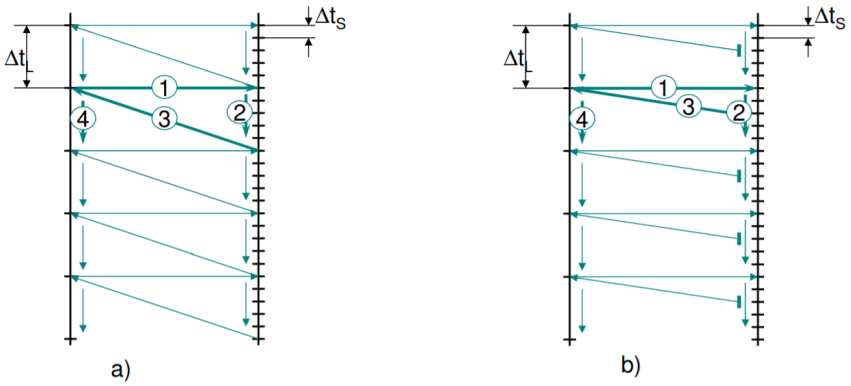

Figure 2.4: Illustration of a fast-first strategy in case of having two subsystems. a) Time-state scheme with instantaneous coupling data. b) Time-state scheme with averaged coupling data[23].

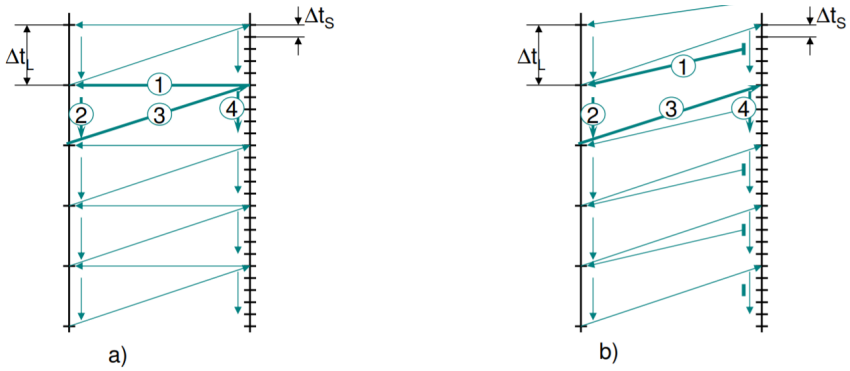

Figure 2.5: Illustration of a slow-first strategy in case of having two subsystems. a) Time-state scheme with instantaneous coupling data; b) Time-state scheme with averaged coupling data[23].

Each of the two strategies, fast-first or slow-first, has its pros and cons. In the fast-first strategy, if the result of the macro time step in the slow subsystem is rejected, at least some of the results in the micro time steps must be recalculated in order to yield an approved result in the macro time step. Thus, in order to avoid many rejected steps, the time step of the fast subsystem must be sufficiently small. This, in turn, leads to more accurate results while increasing the overall simulation time.

On the other hand, if the slow subsystem is simulated first, the time consumption penalty for not achieving a convergent result in the fast subsystem is negligible. This is due to the macro time step being much larger than the micro time step in general. However, extrapolating the variables in the slow subsystem leads to extrapolation error, which increases proportionally with the macro time step[24]. Note that when the simulation of the fast subsystem is initiated in the slow-first strategy, the corresponding values from the

slow subsystem at each micro time step is not available. The simplest way to obtain these values is by using linear interpolation[6]. On the other hand, when using the fast-first strategy, the values of the slow subsystem can be extrapolated from the previous time step.

2.3.2 Predictor-Corrector

The slow-first strategy, as shown in Fig. 2.5, relies on calculating the slow subsystem first followed by the fast subsystem until reaching the same time step. This strategy assumes that the obtained solution is accurate enough without further inspection. However, in order to ensure overall accuracy, a predictor-corrector method can be used instead of a direct slow-first strategy. An example of a predictor-corrector method is the Adams-Bashforth method, which is the matter of discussion in this subsection[25].

The integration procedure implemented for each subsystem, based on Adams-Bashforth method, consists of prediction, evaluation, correction, and evaluation (PECE in short) stages[25]. Considering the slow and fast step sizes ΔT and $\Delta\tau$, respectively, the value of an arbitrary slow component $x(t)$ is predicted first at $t = t_p + \Delta T$, where t_p is the time at previous step. Then the fast subsystem is iterated r number of times with step size $\Delta\tau$, where $\Delta T = r\Delta\tau$. The PECE procedure is used at each time step for both the fast and the slow subsystem. The value of each variable in the slow subsystem $x(t)$ at each intermediate fast step at $t_p < t < t_p + \Delta T$ is found using linear interpolation. The same values are also used in the correction stage for the fast subsystem. The output from the fast subsystem at $t = t_p + \Delta T$ is then used in the correction stage of the slow subsystem[25]. An example of a complete multirate integration algorithm based on the fourth-order Adams-Bashforth predictor-corrector method is presented in[25].

The idea behind the approach in [25] is to provide an initial guess using Adams-Bashforth explicit formula. This is then used to develop an iterative solution for the corrector part based on Adams-Moulton implicit formula. The iterations are carried on until two successive outputs from the corrector part meet certain convergence criteria[25]. In contrast to the slow-first strategy, the predictor-corrector method can be time consuming, albeit a more accurate one. Since the predictor-corrector method is based on iterations between the subsystems until all convergence criteria are met, it can be considered to belong to the fully-dynamic coupling class.

2.3.3 Step-Skipping

The slow/fast-first and predictor-corrector strategies depend on saving data for few time steps in each subsystem before moving on to the other subsystem, as discussed earlier. The two coupling strategies, although effective in many cases, are not ideal when it comes to very large systems. The reason behind this is that in a very large spatial domain, such as in the case of a petroleum reservoir, the data regarding the variables in each grid cell is saved at each time step. This means that the larger the spatial domain, the more data that must be stored. Hence, these two strategies can be unpractical for the use in reservoir simulations due to memory limitation.

In order to bypass the memory limitation issue, all the subsystems can be simulated using a single, but varying, time step dictated by the fastest changing subsystem. This means that only the data from the previous time step is needed for each subsystem. For example, assume there are four subsystems A, B, C and D each with different time scale except for B and C sharing the same time scale. It is assumed there is only one variable in each subsystem. The subsystems B and C experience change more rapidly than D, which in turn change more rapidly than A. The time step in the system is defined by its fastest subsystems, B and C in this case, see Fig. 2.6. Since the rate of change of D and A, or the gradient of D and A, are lower than B and C, only B and C are calculated at the first time step t^1. In the second time step t^2, D is calculated in addition to B and C knowing that sufficient changes have occurred in D. Last, A is also calculated at t^3 in addition to all the other subsystems. This indicates that A is the slowest changing subsystem in the entire system.

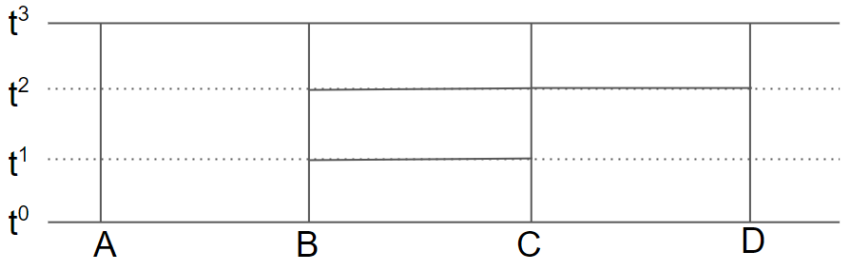

Figure 2.6: Step skipping approach.

If no significant changes occur in a subsystem since the last time step, then calculations are skipped in that particular subsystem (not updated). In this case, the value of each variable in the subsystem from the last updated time step is used when communicating with the other subsystems. Hence, such type of strategy is called step-skipping in this study. It is worth mentioning that if the gradient of the fastest subsystem becomes lower throughout simulation time, the time step t can become larger.

Chapter 3

Determining Time Constants in a Multiphysics Problem

3.1 Time Constant in Multirate Approach

Time constant, or characteristic time, is a term used in lumped system analysis to determine the response of a system to a step change. An example of such system is dipping a cube of metal into a boiling water. Assuming that the temperature in the room and the boiling water is 0°C and 100°C, respectively, the time constant of the heating process of the metal in this case is the time it takes for the metal to reach 63 degrees, which is 63% of 100 degrees. A large time constant in this case means it takes long time for the metal to become warmer and vice versa. In other words, the time constant tells how fast changes occur within a process or a subsystem. It can be used as a tool to differentiate between fast and slow subsystems in a multiphysics problem. A time constant must always be related to a certain process or a subsystem, otherwise its definition becomes ambiguous. This chapter presents methods to determine the time constant of the processes in a system. In this study, the terms time constant and characteristic time are used interchangeably and their value is defined uniquely in each case. Also, the definition of time constant is not restrict to 63% of the process time as mentioned earlier. In other words, the time constant is analogous to the characteristic length used in calculating Reynolds number, which is defined uniquely in each case.

Mathmatically speaking, the idea behind lumped systems is to reduce continuous PDEs in time and space of a physical system into ODEs. A typical solution of an arbitrary ODE function $f(t)$ takes the form $f(t) = Const \cdot exp(-t/\tau_c)$, where τ_c is the variable defining the time constant of the process in hand. The main objective of using τ_c is to obtain a quantitative comparison between the rate of change of different subsystems in a system.

The ratio R_c is introduced in order to determine whether or not a multirate approach must be used based on a predefined criterion or threshold. R_c is defined as the ratio of time constant in the slow subsystem to its corresponding value in the fast subsystem, or $R_c = \tau_c(slow\ subsystem)/\tau_c(fast\ subsystem)$, and is always more than one ($R_c > 1$). In case of having only two processes, the slow subsystem is the process with the highest time constant. The following three approaches are used when determining R_c in this study:

- Domain based: In a fluid flow problem, for instance, the domain based approach takes the entire length of the domain into consideration in addition to the time it takes for the flow to cover the domain. Hence, the whole domain is treated as one entity.
- Cell based: In a cell based approach the temporal and spatial steps Δt and Δx, in case of one dimensional probem, are used as basis for calculating R_c.
- Frequency based: In a frequency based approach, the wave length is used as the characteristic length, while the time constant is defined here as the time it takes for an entire wave length to travel a distance equal to the wave length itself.

There is no theory that dictates when to split a system into several subsystems based on a certain value of R_c. In other words, the question of whether or not to use multirate approach is up to the user to decide. It should be noticed that the time constant approach, or using R_c, is just a quantitative approach to help engineers with choosing a suitable combination of multirate concepts to solve the problem in hand. Hence caution must be exercised when splitting a system into fast and slow subsystems based on R_c. In order to utilize the full potential of the approach, the overall physics along with the interactions in the problem must be understood. The following sections in this chapter present methods to determine the time constant of different processes in a system.

3.2 Splitting Parts

Consider the one dimensional advection-diffusion equation with temperature Θ as the transported variable

$$\frac{\delta\Theta}{\delta t} + a\frac{\delta\Theta}{\delta x} = K\frac{\delta^2\Theta}{\delta x^2}. \tag{3.1}$$

Eq.(3.1) contains the following three terms form left to right: time derivative, advective transport with constant advection velocity a and the diffusive term where K is the thermal conductivity. Since there are two distinct processes in the system, advection and diffusion, Eq.(3.1) can be split into two parts correspondingly, hence the name splitting parts. This

is in order to detect the time constant of each process without interference from the other process. To achieve this, the value of a and K is set to zero in each case as following

$$\frac{\delta\Theta}{\delta t} + a\frac{\delta\Theta}{\delta x} = 0, \tag{3.2}$$

$$\frac{\delta\Theta}{\delta t} = K\frac{\delta^2\Theta}{\delta x^2}. \tag{3.3}$$

As a result, Eq.(3.2) becomes an advection equation. On the other hand, Eq.(3.3) is known as the 1D diffusion equation with the characteristic time $\tau_c = L^2/(K\pi^2)$, where L is the characteristic length.

Using the following values, as an example, $\Delta x = 0.045\,\mathrm{m}$, $L = 10\,\mathrm{m}$, $a = 7\,\mathrm{m/s}$, $\Delta t = 0.005\,\mathrm{s}$, $K = 0.59\,\mathrm{W/(mK)}$ (thermal conductivity of water), the ratio R_c can be calculated using the domain and cell based approaches as following:

- Domain based: The time it takes for Θ to cover the entire domain, i.e. the characteristic time of the advection process, is $10\,\mathrm{m}/7\,(\mathrm{m/s}) = 1.42\,\mathrm{s}$. For the diffusion process, the time constant becomes $10^2/(0.59\pi^2) = 17.17\,\mathrm{s}$. Hence, considering the advection and diffusion terms to be the fast and the slow subsystem, respectively, the ratio R_c is equal to $17.17\,\mathrm{s}/1.42\,\mathrm{s} \approx 12$.

- Cell based: In the cell based approach, the time constant for the advection process is simply $\Delta t = 0.005\,\mathrm{s}$. For the diffusion process, on the other hand, the characteristic length L is now equal to $\Delta x = 0.045\,\mathrm{m}$. Thus, the time constant of the advection process becomes $0.045^2/(0.59\pi^2) = 0.0003\,\mathrm{s}$. Since the time constant of the diffusion process is less than the advection one, the diffusion process in considered to be the fast subsystem in this case. The ratio R_c for the system is now $0.005\,\mathrm{s}/0.0003\,\mathrm{s} \approx 17$.

The conclusion is that the less the characteristic length L, the more dominant the diffusive effects become. This is analogous to Reynolds number as viscous effects becomes more dominant with decrease in characteristic length, which is the diameter of the pipe in case of pipe flow. Although both approaches lead to R_c values of the same order of magnitude, the domain based approach is more accurate since thermal diffusion is a macroscopic effect. Thus, the slow process in this system is the diffusion process and the value of R_c is ≈ 12.

It is worth mentioning that in a diffusion process, the initial condition can play a significant role especially if there are high gradients initially. This to due to the second derivative presented in the diffusion term that is sensitive to high gradients. The effect of the initial

condition is not taken into account when using the splitting approach as presented in this section. In order to include the initial condition, an another approach based on Fourier transformation can be used in the case of having large gradients initially, see next section.

3.3 Fourier Transform

Consider now Eq.(3.1) with the initial condition $\Theta(x,0)$ as following

$$\frac{\delta\Theta(x,t)}{\delta t} + a\frac{\delta\Theta(x,t)}{\delta x} - K\frac{\delta^2\Theta(x,t)}{\delta x^2} = 0 \quad , \quad \Theta(x,0) = \sin(x). \tag{3.4}$$

Instead of splitting the equation into one advection and one diffusion part, the entire equation is solved using Fourier transform instead. Fourier transform is used here to transform a one dimensional linearized PDE into an ODE in order to obtain the time constant of each individual process in the system[26]. The approach is especially useful when it comes to more sophisticated systems containing many processes. The idea behind such approach is that the spatial domain x is transformed to the frequency domain ω[27]. Applying Fourier transform on Eq.(3.4) yields

$$\frac{\delta\hat{\Theta}(\omega,t)}{\delta t} + i\omega a\hat{\Theta}(\omega,t) - (i\omega)^2 K\hat{\Theta}(\omega,t) = 0, \tag{3.5}$$

where $\hat{\Theta}$ is Θ as in Eq.(3.4) but now in frequency domain. Notice that Eq.(3.5) is an ODE which can now easily be solved by integrating in time

$$\hat{\Theta}(\omega,t) = e^{-(ai\omega+K\omega^2)t}\hat{\Theta}(\omega,0). \tag{3.6}$$

Using the initial condition given in Eq.(3.4), the term $\hat{\Theta}(\omega,0)$ in Eq.(3.6) becomes equal to the Fourier transform of $\sin(x)$, i.e. $\hat{\Theta}(\omega,0) = \mathcal{F}(\sin(x))$. The solution of $\hat{\Theta}(\omega,t)$ in the spatial domain can now be obtained by employing the inverse Fourier transform on Eq.(3.6)

$$\Theta(x,t) = \frac{1}{2}e^{-Kt}i[e^{-i(x-at)} - e^{i(x-at)}]. \tag{3.7}$$

Using the relation $\sin(x-at) = \frac{1}{2i}(e^{i(x-at)} - e^{-i(x-at)})$ from Euler's formula for complex potentials, Eq.(3.7) can now be written as

$$\Theta(x,t) = -i^2\sin(x-at)e^{-Kt} \ = \sin(x-at)e^{-Kt}. \tag{3.8}$$

Eq.(3.8) reveals two distinct time constants merging obviously from the advection term and diffusion term as $\sin(x-at)$ and e^{-Kt}, respectively. The time constant τ_c of the diffusion term is therefore 1/K. Using the same values for the variables as in Section 3.2,

the time constant of the diffusion process becomes 1.7 s. On the other hand, since Fourier transform is inherently frequency based, the characteristic length associated with the advection process is therefore the wave length of $\sin(x - at)$ (see Section 3.1), which is 2π. The characteristic time of the advection process using the frequency based approach is therefore $2\pi\,\mathrm{m}/7\,(\mathrm{m/s}) = 0.9\,\mathrm{s}$. The ratio R_c of the system is now $1.7\,\mathrm{s}/0.9\,\mathrm{s} \approx 2$.

It must be pointed out that the Fourier transform approach requires an oscillatory initial condition with a certain frequency, which is not always the case in real life scenarios. However, a non-oscillatory initial condition can always be approximated by an oscillatory function, hence retaining the generality of the Fourier approach.

3.4 Eigenvalue Analysis

As mentioned in the introduction to this chapter, the time constant of a process modelled by an ODE is obtained by τ_c from its solution. The same analogy is used in case of a more complex system involving many linear ODEs. However, this time the time constants are obtained by taking the inverse of the eigenvalues from the solution of the linearized system[28]. To illustrate this, consider a house with an attic, main floor and a basement as in Fig.3.1

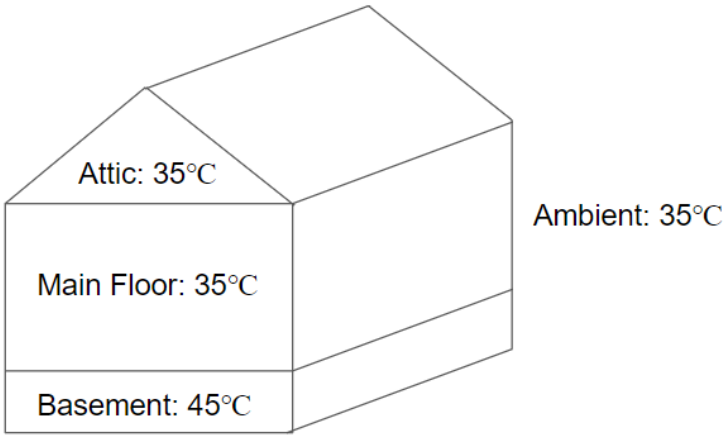

Figure 3.1: Initial temperatures in the system.

Note that the variables used in this section are only valid for this section and can have different meanings in the rest of the study. The temperature in the attic, main floor and the basement in this section are denoted by $z(t)$, $y(t)$ and $x(t)$, respectively, and time t is given in hours. The initial temperatures are as shown in Fig. 3.1. An electric heater, providing 20°C rise per hour, is turned on in the main floor with thermostat set for 100°C. Newton's law of cooling is used to calculate the temperature changes in the system as following

$$\textit{Temperature rate} = k(\textit{Temperature difference}), \tag{3.9}$$

where k is the insulation constant. In other words, the lower the value of k, the more insulation is available and therefore less heat exchange. The following five boundaries are defined with their corresponding value of insulation constant:

- $k_0 = \frac{1}{2000}$: The basement walls and the floor against the ground.
- $k_1 = \frac{1}{2000}$: The wall between the basement and the main floor.
- $k_2 = \frac{1}{4}$: The walls in the main floor.
- $k_3 = \frac{1}{4}$: The wall between the main floor and the attic.
- $k_4 = \frac{1}{2}$: The attic walls and the ceiling against ambient air.

Notice that the values of k_0 and k_1 are much less than k_2, k_3 and k_4, which means that the basement is almost fully insulated. Having defined the initial temperatures in the system along with the insulation constants, the system of equations describing the changes in temperatures based on Eq.(3.9) can be written as

$$\begin{aligned} \dot{x} &= 45k_0 - x(k_1 + k_0) + yk_1, \\ \dot{y} &= xk_1 - y(k_1 + k_2 + k_3) + 35k_2 + zk_3 + 20, \\ \dot{z} &= yk_3 - z(k_3 + k_4) + 35k_4, \end{aligned} \tag{3.10}$$

or as following in matrix form

$$\begin{bmatrix} \dot{x} \\ \dot{y} \\ \dot{z} \end{bmatrix} = \begin{bmatrix} -(k_0 + k_1) & k_1 & 0 \\ k_1 & -(k_1 + k2 + k3) & k_3 \\ 0 & k_3 & -(k_3 + k_4) \end{bmatrix} \begin{bmatrix} x \\ y \\ z \end{bmatrix} + \begin{bmatrix} 45k_0 \\ 35k_2 + 20 \\ 35k_4 \end{bmatrix}. \tag{3.11}$$

The variables $\dot{x}$, $\dot{y}$, and $\dot{z}$ represent the time derivatives of their corresponding variables x, y and z. For the sake of compactness, the values of the insulation constants are inserted and the homogeneous solution, denoted by the subscript h, of the system of ODEs in (3.11), can now be written as

$$\begin{bmatrix} x_h \\ y_h \\ z_h \end{bmatrix} = Const_1 e^{\xi_1 t} V_1 + Const_2 e^{\xi_2 t} V_2 + Const_3 e^{\xi_3 t} V_3. \tag{3.12}$$

The variables ξ_j,V_j and $Const_j$ for $j = 1, 2, 3$ represent the eigenvalues, eigenvectors and the constants of the system, respectively. The subscript j refers to the amount of variables

in the system, which is three (x, y and z). In order to find the particular solution, the equation system in (3.10) is solved by setting the time derivatives to zero, indicating a steady state condition. The particular solution, denoted by the subscript p, is shown to be

$$\begin{bmatrix} x_p \\ y_p \\ z_p \end{bmatrix} = \begin{bmatrix} 53.48 \\ 61.97 \\ 43.97 \end{bmatrix}. \tag{3.13}$$

By inserting the values of the insulation constants in (3.12), the following is obtained

$$V_1 = \begin{bmatrix} 0.0003 \\ -5.5261 \\ 0.8504 \end{bmatrix} \quad ; \quad \mathrm{V}_2 = \begin{bmatrix} 0.0012 \\ -0.8504 \\ -0.5261 \end{bmatrix} \quad ; \quad \mathrm{V}_3 = \begin{bmatrix} 1 \\ 0.0012 \\ 0.0004 \end{bmatrix},$$

$$\xi_1 = -0.9046 \quad ; \quad \xi_2 = -0.3459 \quad ; \quad \xi_3 = -0.001,$$

$$Const_1 = 1.80 \quad ; \quad Const_2 = 19.96 \quad ; \quad Const_3 = -8.50.$$

The final solution of the system including both the homogeneous and particular solutions can therefore be written as

$$\begin{aligned} x(t) &= 0.00054e^{-0.9t} + 0.239e^{-0.34t} - 8.50e^{-0.001t} + 53.48, \\ y(t) &= -9.94e^{-0.9t} - 16.97e^{-0.34t} - 0.01e^{-0.001t} + 61.97, \\ z(t) &= 1.53e^{-0.9t} - 10.50e^{-0.34t} - 0.003e^{-0.001t} + 43.97. \end{aligned} \tag{3.14}$$

The eigenvalue approach, unlike the Fourier transform and splitting part approaches, does not yield a unique time constant for each process. The reason for this is that different processes in a system of ODEs are intertwined, therefore, the solution must take into consideration all the processes in the system. However, the eigenvalues can still be strongly associated with certain processes. Hence, the method can be useful when determining the time constants of different processes in a system.

It can be observed from (3.14) that the two first terms to the left of equation $x(t)$ are negligibly small compared to the third term (small coefficients). In addition, the eigenvalue ξ_3 is significantly small compared to ξ_1 and ξ_2. This indicates that the change in the initial temperature in the basement is very small over time, which is expected knowing that the basement is almost fully isolated. At the same time, the third term from the left of equations $y(t)$ and $z(t)$ are also negligible compared to the first and the second terms. The only explanation to this is that the third terms must be associated with temperature change in the basement, which is very small due to it being fully insulated. In other words, the eigenvalue ξ_3 and eigenvector V_3 are strongly associated with the temperature

change in the basement. Hence, it can be concluded that the time constant of $x(t)$ is equal to $1/\xi_3 = 1000\,\mathrm{s}$.

Following the same line of reasoning, ξ_1 is larger than ξ_2, which means that the change in temperature associated to the process related to ξ_1 must also be larger than the one related to ξ_2. Since there is a heater turned on in the main floor, ξ_1 must therefore be related to $y(t)$. Thus, the time constants of the processes $y(t)$ and $z(t)$ are 1.1 s and 2.9 s, respectively. Needles to say, the slow subsystem in this case is the temperature change in the basement $x(t)$, while the fast subsystems are the temperature change in the main floor $y(t)$ and the attic $z(t)$. In order to proof that the time constants designated to the three processes are physical, the temperature in each region is tested at their corresponding value of time constant. This time using the definition of 63% of the total time. The following results are obtained

$$\begin{bmatrix} x_{1000} \\ y_{1.1} \\ z_{2.9} \end{bmatrix} = \begin{bmatrix} 50.35 \\ 46.59 \\ 40.16 \end{bmatrix}. \tag{3.15}$$

Taking 63% of the difference between the temperature at steady state and initial condition (to find the temperature at the designated time constant), the theoretical temperature in $x(t)$, $y(t)$ and $z(t)$ is 50.34°C, 51.99°C, and 40.65°C, respectively. In other words, the theoretical temperature in $x(t)$ and $z(t)$ show almost perfect alignment with the results obtained in (3.15). There is however a deviation of 5.4°C when it comes to $y(t)$. The reason for this lies in $y(t)$ being connected to all the other regions, which makes process $y(t)$ even more intertwined with the system. This in turn leads to an eigenvalue ξ_1 that is more affected by the other processes. It can therefore be concluded that the less a process is in interaction with the other processes in a given system, the more strongly an eigenvalue can be associated to that specific process.

The ratio R_c between $x(t)$ and $y(t)$ is $1000\,\mathrm{s}/1.1\,\mathrm{s} \approx 909$, and between $x(t)$ and $z(t)$ is $1000\,\mathrm{s}/2.9\,\mathrm{s} \approx 345$. Last, the value of R_c between $z(t)$ and $y(t)$ is $2.9\,\mathrm{s}/1.1\,\mathrm{s} \approx 3$.

3.5 Order of Magnitude

Determining whether or not a subsystem is fast or slow can also be deduced using qualitative analyses such as the order of magnitude approach. This approach is widely used in physics and mathematics to eliminate terms that are of significantly lower order of magnitude than the other terms in the system. It should be noticed that the variables

used in this section are only valid for this section and can have different meanings in the rest of the study.

The example case used here to demonstrate the approach is inspired from the world of ecology where two predators, x_1 and x_2, compete for the same prey S. This can be modelled using the following set of ODEs to describe the predator-prey dynamics[29]

$$\begin{aligned} \dot{S} &= \gamma S(1 - \frac{S}{K}) - \frac{m_1}{y_1}\frac{x_1 S}{a_1 + S} - \frac{m_2}{y_2}\frac{x_2 S}{a_2 + S}, \\ \dot{x_1} &= \frac{m_1 x_1 S}{a_1 + S} - d_1 x_1, \\ \dot{x_2} &= \frac{m_2 x_2 S}{a_2 + S} - d_2 x_2. \end{aligned} \tag{3.16}$$

The variables $\dot{S}$, $\dot{x_1}$ and $\dot{x_2}$ represent the time varying population density of the prey and the predators, respectively. The variables with subscripts 1 and 2 refer to predator x_1 and x_2. Furthermore, y_1 and y_2 are the yield factors for the predators feeding on the prey; a_1 and a_2 are the half saturation constant for the predators; $m_1, m_2 > 0$ and $d_1, d_2 > 0$ are the birth and death rates of the corresponding predators, respectively; and $\gamma > 0$, $K > 0$ are the intrinsic growth rate and the carrying capacity of the prey, respectively.

In order to analyse the system with minimum number of variables, the equation system in (3.16) is non-dimensionalized and the following nonlinear system of ODEs is obtained

$$\begin{aligned} \dot{x} &= x(\frac{m_1 z}{\beta_1 + z} - d_1), \\ \dot{y} &= y(\frac{m_2 z}{\beta_2 + z} - d_2), \\ \dot{z} &= \frac{1}{\epsilon} z(1 - z - \frac{m_1 x}{\beta_1 + z} - \frac{m_2 y}{\beta_2 + z}). \end{aligned} \tag{3.17}$$

The newly introduced variables in (3.17) are defined as

$$\epsilon = \frac{1}{\gamma}, \quad \beta_1 = \frac{a_1}{K}, \quad \beta_2 = \frac{a_2}{K}, \quad x = \frac{x_1}{\gamma y_1 K}, \quad y = \frac{x_2}{\gamma y - 2K}, \quad z = \frac{S}{K}, \tag{3.18}$$

where x, y and z are time dependent unknown functions. The intrinsic growth rate of the prey γ is considered to be very high ($\epsilon << 1$). As a consequence, the changes to the variable z corresponding to the prey population becomes much faster than the other two variables corresponding to the two predators. This is due to the order of magnitude of $\frac{1}{\epsilon}$ being much larger than one, which is the coefficient of the variables x and y in (3.17). In other words, the prey population is considered to be the fast subsystem while the two predator populations are the slow subsystems.

The advantage of using the order of magnitude approach is that it is very general and does not need heavy mathematical analysis such as in the case of the Fourier transform approach. However, the downside is that no quantitative numbers such as τ_c and R_c can be obtained.

3.6 Self-Adjusting Methods

There are many methods in the literature that help in determining the most efficient time step size for each subsystem based on for instance a local error estimator. These methods are often referred to as self-adjusting methods. In these kind of methods, all the subsystems are initially given the same tentative global time step size. Then an error estimator is used to mark the subsystems with local error larger than a specified tolerance. These subsystems are then given a shorter time step until the error is low enough[30]. In other words, the method becomes self-adjusting while being able to differentiate between the different time scales presented in the system. As a consequence, no manual analysis such as in the approaches discussed earlier is needed to determine whether a subsystem is fast or slow. Hence, these methods are especially robust when it comes to systems where the time scale of the subsystems change throughout simulation time, i.e. when R_c is not constant, as no intervention is needed by the user. In addition, simulation platforms that are based on these methods to determine the time step in each subsystem do not need highly skilled operators (since the process is automated). These advantages is what renders self-adjusting methods the primary choice of many commercial simulators such as OpenFOAM[31] and Brilliant. A step by step procedure for implementing a self-adjusting method is presented in[30].

3.7 The Main Six Characteristics of Multirate Approach

Using multirate approach to solve a multiphysics problem requires thorough understanding of the physics involved. Table 3.1 can be helpful to obtain an overview of the problem in hand. The table opens the opportunity for the user to discuss different methods and approaches that can be used in a multiphysics simulation. The concepts and approaches discussed in Chapters 2 and 3 reveal in total six characteristics attached to multirate approach as shown in the table below.

Table 3.1: The main six characteristics of a multirate approach.

Part 1

Strength of coupling	Coupling strategies	Coupling between physics
Strong	Fast-First vs. Slow-First	Geometric
Weak	Predictor-Corrector	Volumetric
	Step-Skipping	

Part 2

Coupling problem	Time constant analysis	Multirate philosophies
Coupled	Splitting parts	Monolithic
Coupled multi-field	Fourier transform	Partitioned
Coupled multi-physics	Eigenvalue analysis	Fractional step
	Order of magnitude	Field variable elimination
	Self-adjusting approach	

Chapter 4

Governing Equations of Well-Reservoir Dynamics

4.1 General Assumptions

In this chapter, the equations governing the fluid flow both in the well and the reservoir are presented and used as basis for the simulations in Chapter 6. The interactions between the two subsystems, the well and the reservoir, are often referred to as well-reservoir dynamics[32]. The major difference between the two subsystems is that, in a reservoir, fluids flow through porous media and the velocity of the flow is found using Darcy's law, hence the name Darcy flow. On the other hand, fluid velocity in a well stream is calculated using Navier-Stokes equation. Such type of flow is therefore referred to as Navier-Stokes flow. The equations presented in this chapter are based on the following assumptions which apply for both subsystems:

- Laminar flow in a single phase (mixture of hydrocarbons).
- No phase changes in the fluid. The flow is always in liquid state.
- Three dimensional in Cartesian coordinates.
- Compressible unless other is mentioned.
- No mass transfer between solid and fluid.
- No chemical reactions.
- Small temperature changes.
- Homogeneous and isotropic porous medium with constant porosity and permeability.

In this study, the flow in the well is assumed to be the fast subsystem, while the flow in the reservoir is regarded as the slow subsystem. Consequently, $\partial\tau$ is used in the former and ∂T in the latter to indicate their respective time derivatives. This assumption will be verified quantitatively in Section 6.3.2.

4.2 Reservoir

The equations in this section are commonly used in reservoir engineering to predict the amount, temperature and composition of hydrocarbons flowing into a well. Unless other is mentioned, the description in this section is taken from the book by Das et al.[33]. It should be noticed that the description in this section is related to the flow in the bulk region of the reservoir and not in the vicinity of the well. The reason for this is that the gradients near the well can be large, which in turn may defy some of the assumptions made while deriving the equations.

4.2.1 Darcy's Law

Darcy's law form the scientific basis of fluid permeability used in earth sciences particularly in hydrogeology[34]. The name comes from the French engineer Henry Philibert Gaspard Darcy (1803-1858). He is well known for his contributions to groundwater flow and for having carried out experiments on flow through filters such as sand, which eventually led to his well celebrated law.

Darcy's law, described by Eq.(4.1), is a generalized relationship for flow in porous media such as soil or a reservoir, see Fig. 4.1 for illustration. It shows that the volumetric flow rate is a function of flow area A_s, difference in fluid pressure, permeability and the dynamic viscosity of the fluid. It may be stated in several different forms depending on the flow conditions. Since its discovery, it has been found to be valid for any Newtonian fluid. However, the law is bound to laminar flow, which is shown to be the case when the Reynolds number is less than unity[35]. The diameter of particles D_p in a porous medium is often used as the characteristic length when determining the Reynolds number. Nonetheless, finding the characteristic length can be challenging in very coarse- grained porous media as the geometry of the particles can become vague.

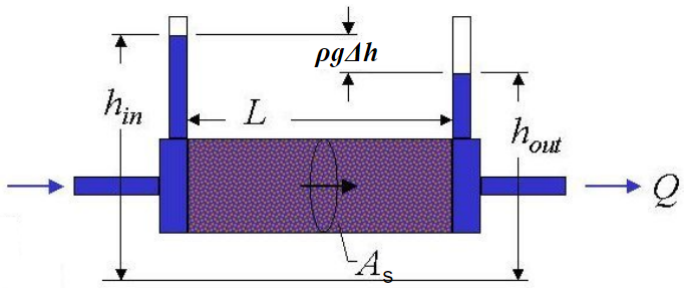

Figure 4.1: A general illustration of one-dimensional flow column in a porous medium as described by Eq.(4.1)[36]. The driving force for the fluid flow arises from the pressure difference between the two points with distance L in between.

$$Q_j = -\frac{\kappa A_s}{\mu}\frac{\rho g \Delta h}{L} = -\frac{\kappa A_s}{\mu}\frac{\partial p}{\partial x_j}. \tag{4.1}$$

The permeability κ represents the ability of a porous medium to transmit fluids. Using dimensional analysis, it can be shown that κ is a function of porosity and particle diameter as shown in the *Kozeny-Carman* relationship[37],

$$\kappa = \frac{D_p^2 \psi^3}{180(1-\psi)^2}, \tag{4.2}$$

where ψ is the total volume porosity, or just porosity, and is defined as V_{fluid}/V_{cv}. V_{fluid} is the volume of the fluid in a control volume, while V_{cv} is the volume of the control volume itself. The velocity q_j in porous media can be obtained from Eq.(4.1) by dividing with A_s on both sides,

$$q_j = -\frac{\kappa}{\mu}\frac{\partial p}{\partial x_j}. \tag{4.3}$$

Hence, the velocity of the flow in porous media can simply be approximated using Eq.(4.3) without having to solve for a momentum equation, assuming that the flow is in a quasi-steady-state condition. However, Eq.(4.3) is based on the bulk flow and not on the exact velocity field as in the case when using Navier-Stokes equation.

4.2.2 Pressure and Mass Conservation

Conservation of mass in porosity flow is captured by the continuity equation as following

$$\frac{\partial(\psi\rho)}{\partial T} + \frac{\partial(\rho q_j)}{\partial x_j} = 0. \tag{4.4}$$

Inserting for q_j from Eq.(4.3), Eq.(4.4) now becomes

$$\frac{\partial(\psi\rho)}{\partial T} - \frac{\partial}{\partial x_j}(\frac{\kappa\rho}{\mu}\frac{\partial p}{\partial x_j}) = 0. \tag{4.5}$$

Since density is a function of only pressure given that temperature changes are small, the first term to the far left in Eq.(4.5) can be expressed as

$$\psi\frac{\partial\rho}{\partial T} = \psi\frac{\partial\rho}{\partial p}\frac{\partial p}{\partial T}. \tag{4.6}$$

Assuming isentropic process due to weak pressure gradients in the reservoir, the pressure derivative of density can be written as[38]

$$(\frac{\partial\rho}{\partial p})\bigg|_{isentropic} = \frac{1}{c^2}, \tag{4.7}$$

where c is the speed of sound. Inserting Eqs.(4.6) and (4.7) into Eq.(4.5) yields the pressure equation,

$$\psi\frac{1}{c^2}\frac{\partial p}{\partial T} - \frac{\partial}{\partial x_j}(\frac{\kappa\rho}{\mu}\frac{\partial p}{\partial x_j}) = 0. \tag{4.8}$$

4.2.3 Energy

Using the first law of thermodynamics as a basis, the equation governing convective and conductive heat transfer in Navier-Stokes flow is given by

$$\frac{\partial(\rho C_p\Theta)}{\partial T} + \frac{\partial(\rho C_p\Theta u_j)}{\partial x_j} = \frac{\partial}{\partial x_j}(K\frac{\partial\Theta}{\partial x_j}). \tag{4.9}$$

The variables C_p and K are the specific heat and thermal conductivity of the fluid, respectively, and u_j is the velocity vector. The following assumptions are applied when deriving Eq.(4.9) :

- Negligible viscous dissipation.
- No shaft work (or devices).
- No heat generation and radioactive fluxes.
- Weak pressure gradients.
- Small changes in C_p.

In order to expand Eq.(4.9) to porous media, a few more assumptions and variables must be introduced. First, the temperature of the fluid and the particular porous medium are considered to be the same, i.e. the solid and fluid phases are in thermal equilibrium at

all time. The thermal conductivity K is now substituted with K_m, which refers to the effective medium conductivity, hence the subscript m. Moreover, the advection term is given the subscript f to indicate that the energy is transferred by the fluid phase. Last, the time derivative is now defined as the change in energy of the medium, hence $(\rho C_p)_m$ is used. The equation of thermal energy in porous media can now be written as

$$\frac{\partial((\rho C_p)_m \Theta)}{\partial T} + \frac{\partial((\rho C_p)_f \Theta u_j)}{\partial x_j} = \frac{\partial}{\partial x_j}(K_m \frac{\partial \Theta}{\partial x_j}). \tag{4.10}$$

The thermal properties $(\rho C_p)_m$ and K_m can be modelled by the simplest correlation between the solid phase, denoted with subscript s, and the fluid phase to that of the porous medium using the rule of mixtures as following

$$K_m = \psi K_f + (1 - \psi) K_s, \tag{4.11}$$

$$(\rho C_p)_m = \psi (\rho C_p)_f + (1 - \psi)(\rho C_p)_s. \tag{4.12}$$

Mixture rules, such as Eqs.(4.11) and (4.12), are based on the assumption that the thermal properties of a porous medium is the weighted average of the thermal properties of both the solid and the liquid phase. Fig. 4.2 illustrates different approaches in finding the thermal conductivity of a porous medium as a function of porosity.

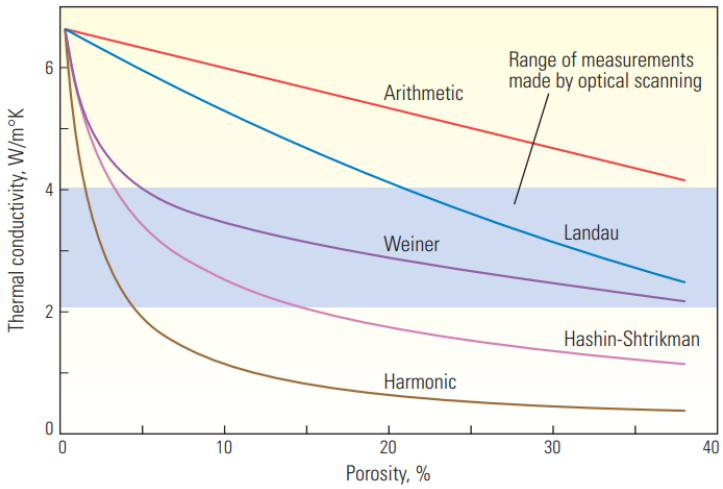

Figure 4.2: Conductivity vs porosity of quartz sandstones[39].

4.2.4 Transport of Species

Transport of species in the context of fluid flow refers to the transport of a solute in a solvent such as salt in water. The concentration C_k, also called mass concentration, is defined as the concentration of a species k in a fluid. The solution in this study is

considered to be free of particulates, which means that the diffusive mass flux $\dot{m}''$ is related to the concentration gradient ∇C_k. In case of having a dilute solution, i.e. low solute concentration, the relationship between the diffusive mass fluxes and the concentration gradient becomes linear. The diffusion coefficient D, which is assumed to be constant, is defined as the mass diffusivity of a solute in a solution. The equation expressing this relationship is similar to the Fourier's law, where heat flux and temperature gradient are coupled together with the proportionality constant K_m. In the context of mass transfer, the relationship is given by Fick's law as following

$$\dot{m}'' = -D\frac{\partial C_k}{\partial x_j}. \tag{4.13}$$

The analogy between mass transfer and thermal energy continues beyond Fick's law to include the governing equations as well. Consider a flow of fluid with a certain amount of dissolved solute, the law governing the transport of the solute is based on the conservation of mass, which yields the following

$$\frac{\partial C_k}{\partial T} + \frac{\partial (C_k u_j)}{\partial x_j} = \frac{\partial}{\partial x_j}(D\frac{\partial C_k}{\partial x_j}). \tag{4.14}$$

Eqs.(4.14) and (4.9) are similar in which the time derivative, advection and diffusion terms are almost the same. The main difference is that the transported quantity is now C_k and the proportionality constant is D. Eq.(4.14) can further be extended for use in porous media by including the effects of porosity and replacing D by D_m to indicate the mass diffusivity in a porous medium. The law governing the transfer of species in porosity flow can now be written as

$$\frac{\partial C_k}{\partial T} + \frac{1}{\psi}\frac{\partial (C_k u_j)}{\partial x_j} = \frac{\partial}{\partial x_j}(D_m\frac{\partial C_k}{\partial x_j}). \tag{4.15}$$

4.3 Well Flow

The flow in a well is similar to an ordinary pipe flow. The only difference is that there is continuous feed of fluids into the well. Following are the equations that govern the flow in a well stream starting from the conservation of mass (Eq.(4.16)), momentum (Eq.(4.17)) and enthalpy (Eq.(4.18)) in addition to the transport of species (Eq.(4.19)).

$$\frac{\partial \rho}{\partial \tau} + \frac{\partial \rho u_j}{\partial x_j} = 0, \tag{4.16}$$

$$\frac{\partial (\rho u_i)}{\partial \tau} + \frac{\partial (\rho u_i u_j)}{\partial x_j} = -\frac{\partial p}{\partial x_i} + \frac{\partial \sigma_{ij}}{\partial x_j}, \tag{4.17}$$

$$\frac{\partial(\rho h_e)}{\partial \tau} + \frac{\partial(\rho u_j h_e)}{\partial x_j} = \frac{\partial}{\partial x_j}(\frac{\mu}{Pr}\frac{\partial h_e}{\partial x_j}), \tag{4.18}$$

$$\frac{\partial(\rho Y_k)}{\partial \tau} + \frac{\partial(\rho u_j Y_k)}{\partial x_j} = \frac{\partial}{\partial x_j}(\frac{\mu}{Sc}\frac{\partial Y_k}{\partial x_j}), \tag{4.19}$$

$$\sum_{k=1}^{N} Y_k = 1. \tag{4.20}$$

The symbol N here refers to the number of different species present in the system. The variable Y_k is used to denote the mass fraction of a species k instead of the concentration which can be written as $C_k = \rho Y_k$. For compressible flow, the pressure can be found using an equation of state, while in case of incompressible flow, the pressure in the well is determined by the pressure of the reservoir at the well-reservoir interface. Furthermore, the cross sectional area of the flow in each control at the interface between the well and the reservoir is of the same size as shown in Fig. 4.3. Numerically speaking, the subsystems are coupled such that the velocity from the reservoir subsystem at the interface, for instance, is used as the velocity at the eastern boundary in the well subsystem when using Eq.(4.17). The eastern boundary of the control volume in the well subsystem lies at the interface between the two subsystems (see Fig. 4.3). On the other hand, the value of each variable from the well subsystem is used at the western boundary in the reservoir control volume at the interface. Hence, the two subsystems are coupled in multiple ways.

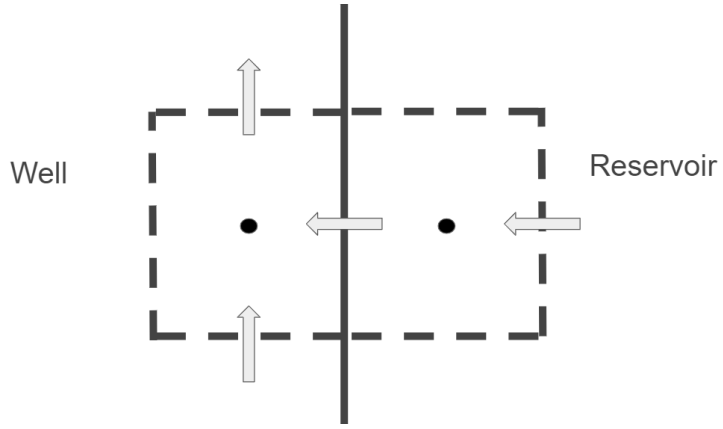

Figure 4.3: Control volumes at the interface between the well and the reservoir. The bold vertical line in the middle indicates the interface between the two subsystems.

Chapter 5

Overview of Physics and Numerical Approaches in a Reservoir

This chapter presents a brief introduction to the effect of ground depth on the pressure and temperature in a reservoir. In addition, an overview of oil recovery process and numerical approaches used to simulate well-reservoir dynamics are given here. The overview in this chapter serves as a basis for the reservoir simulations presented in Chapter 6. See Appendix A for more general information about oil and gas reservoirs.

5.1 Reservoir Pressure and Temperature

The total fluid pressure measured at a point in a reservoir is the sum of two components, the overburden pressure and the pore-fluid pressure. The overburden pressure is generated by the weight of the column of rock or fluids above the point where the pressure is measured. The pore-fluid pressure, on the other hand, is the intrinsic pressure of the fluid being in a confined space with certain porosity[40]. The overburden pressure increases linearly with the depth as shown in Fig. 5.1. The gradient of the pressure in relation to depth varies with the density of the fluid in the region.

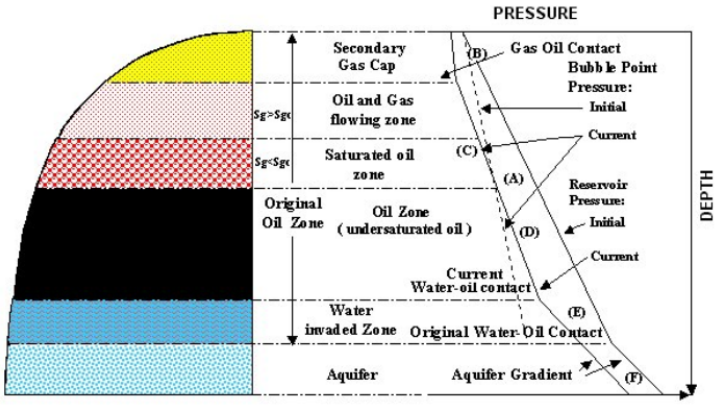

Figure 5.1: Pressure profile along the depth of a reservoir. The different fluid regions are not of interest here[41].

Looking at Fig. 5.2, it is shown that the lowest pressure in a reservoir at a certain depth is at the interface with the well. The gradient of the pressure becomes larger the closer the distance is to the well. This is due to the pressure in the well being the lowest in the entire system in case of having a production well (does not apply for an injection well, see Appendix A.4), which is the type of well that is of concern in this study.

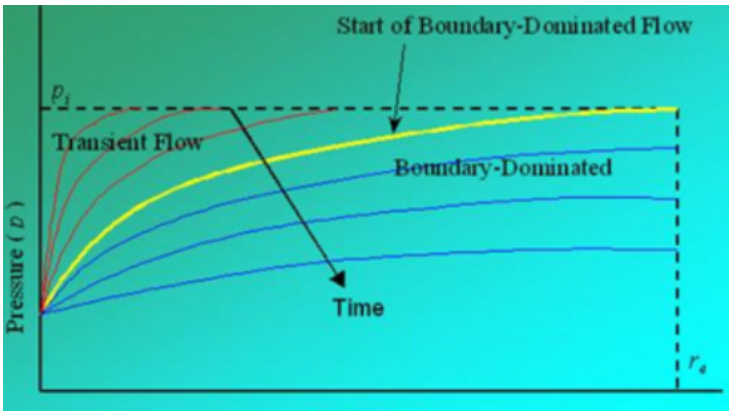

Figure 5.2: Illustration of pressure development in a reservoir throughout time. The horizontal axis refers to the distance from the well (from the left) into the reservoir[42].

Throughout the life time of a reservoir, the overall pressure can be reduced significantly in comparison with the temperature, which in turn may lead to phase changes. Fig.5.3 shows that fluids in liquid phase start evaporating when the bubble point is reached, while gases on the other hand, start changing phase over to liquid at the dew point.

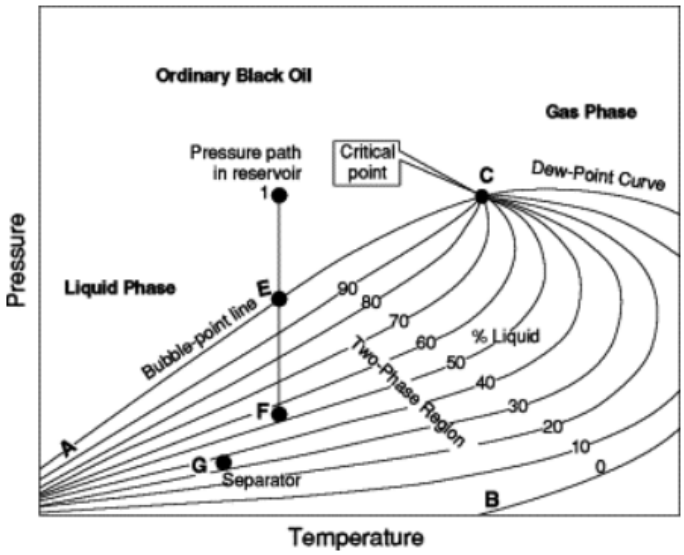

Figure 5.3: Temperature-pressure phase diagram[43].

The temperature in a reservoir is mainly affected by the proximity to the earth's mantle in addition to the thermal properties of the formations in the reservoir, such as heat conductivity and heat capacity[40]. Hence, the geothermal gradient varies from region to another, but the difference within a certain region with the same thermal properties is small. In many reservoirs, the gradient usually ranges between 0.6° F and 1.6° F per 100 ft of increase in depth (11°C/km - 29°C/km) as shown in Fig. 5.4[40]. Regions where the geothermal activity is high can experience gradients as high as 4° F per 100 ft of depth increase (72°C/km).

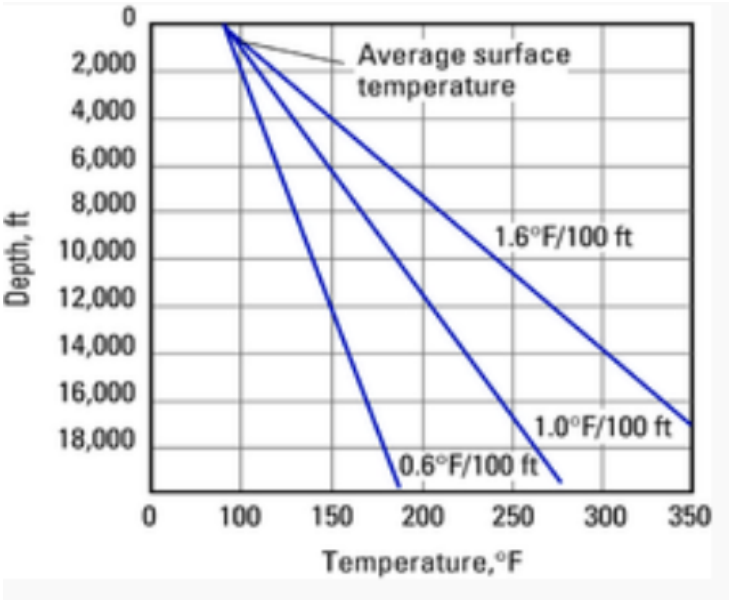

Figure 5.4: Temperature gradients along depth of three different regions in a reservoir[40].

5.2 Qualitative Analysis of Well-Reservoir Dynamics

In this section, the physics and the interactions between the different processes in a well-reservoir system is analysed and discussed quantitatively.

5.2.1 General Overview

Fig. 5.5 illustrates the average pressure in a reservoir (blue line) throughout a period of 68 years. It can be seen that the average pressure suddenly increases after a period of approximately 11 years, which indicates that a secondary recovery method is used (see Appendix A.4). Notice that the pressure in the reservoir is only decreased by 50% during the first 11 years even though the pressure gradient is the highest in the first few years. This leads to the conclusion that the change in the average pressure in a reservoir is slow over time, i.e. can be assumed to be constant for short period of time. As a matter of fact, reservoir processes such as pressure respond to changes on a timescale from hours to decades, whereas processes that take place in a well respond to disturbances in the order of seconds to tens of minutes[32].

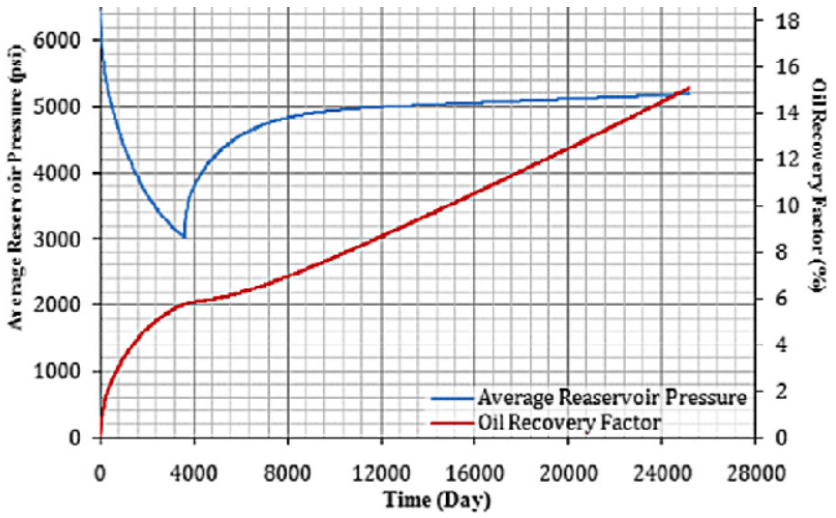

Figure 5.5: Pressure vs. time in a typical reservoir[44]. The oil recovery factor is not of concern here.

As the flow in a reservoir reaches a well, a new set of laws governing its physics take over as mentioned in Chapter 4. Typically, fluids in a well are advected much faster than in the case of flow in a reservoir. This is due to the lack of resistance imposed by the porous media (in a reservoir). As a consequence, the time scale of the flow in a reservoir is much higher than in a well. The difference in the time scales lead to challenges, or looked at differently, may lead to possibilities if the system is understood and its characteristics are exploited.

When a new well is drilled into a reservoir, the initial pressure gradient is at its highest between the reservoir and the well. This pressure gradient leads to the flow of hydrocarbons that transport mass, species and energy. These three variables are transported by Darcy's velocity, hence their time scale is distinguished from the time scale of pressure changes in a reservoir. The latter variable is considered to be the slowest changing based on Fig. 5.5. In addition, fluid flow in a reservoir is the major form of heat transport, which in turn, is an important aspect of determining the composition of each phase as shown in Fig. 5.3.

5.2.2 Coupling between the Subsystems

Choosing a suitable coupling approach between the two subsystems depends on the size scale of the reservoir itself. For instance, according to a paper published by the University of Stavanger in 2014, the estimated reserves of Johan Sverdrup field, that is scheduled to start-up in 2019, is between 1.8 to 2.8 billion barrels or 214 million m^3 to 333 million m^3 of oil[45]. Therefore, the step-skipping approach is the most suitable approach (see Subsection 2.3.3). The question that arises at this point is to determine which variables that must be calculated at each time step, and which others that can be skipped.

As discussed earlier, pressure changes in a reservoir can be considered to be constant over short periods of time. As a consequence, the change in mass flow, concentration of fluids and temperature in a well subsystem becomes small. This is due to the pressure gradient being the main driver of the flow into the well according to Darcy's law. In other words, less flow leads to less transport of mass, species and energy. Moreover, the bulk advection velocity in a well, although slow changing, accounts for most of the transport of both energy and species aside from heat conduction and mass diffusion. These two variables must be monitored closely if a simulator is to predict the composition of the different phases at the outflow of a well.

Since the pressure in a reservoir is always higher than in a well as mentioned earlier, the flow is said to be one directional (into the well). As a result, the three variables, momentum, mass flow and transport of species in a well subsystem do not affect the conditions in a reservoir significantly (still coupled in both directions). This is however not the case with energy transport as the flow in a well can exchange heat with the reservoir around due to temperature gradients along the depth, see Fig 5.4. In other words, the transport of energy in a well is coupled more strongly to the reservoir around than the three other variables (mass flow, momentum and transport of species). In practice this means that

the energy transport in a well must be calculated more often than the other three slow changing variables when using the step-skipping approach. This would be efficient in case of having an incompressible single phase flow where there is not much thermodynamics involved. On the other hand, and in case of having a multiphase flow, then all the three other variables must be calculated as often as the energy transport. The reason for this is that changes in temperature may directly lead to changes in the composition and density of each phase. In other words, the more thermodynamics is involved, the more complex the flow becomes, and therefore, all the variables in a well subsystem must be calculated simultaneously.

Notice that the equations of energy (Eq.(4.18)) and species (Eq.(4.19)) transport in a well subsystem both contain a diffusion term to the far right hand side. These terms can be small compared to the advection terms. However, including the diffusion terms is beneficial not only in having a more accurate model, but also in achieving a better numerical stability[46]. Furthermore, since a reservoir simulation model is based on seismic data that are more unreliable with increasing depth[47], more and more assumptions can be made to simplify the flow proportionally with the depth. The reason for this is that no accuracy is guaranteed even if the entirety of the system is simulated meticulously, as the initial values might be wrong in the first place[10]. Last, based on the discussion above, four different time constants/scales (relative rate of change over time) can be recognized in a well-reservoir system, see Table 5.1.

Table 5.1: Relative rate of change of the variables in a well-reservoir system over time. The flow is assumed to be incompressible and in single phase under normal production conditions. In the case of compressible flow, the time scales "fast" and "fastest" can be merged to only one time scale.

Relative rate of change over time	Well	Reservoir
Slowest		Pressure
Slow		Darcy's velocity, transport of energy, species and mass
Fast	Change in momentum, transport of species and mass	
Fastest	Transport of energy	

5.3 Numerical Approaches to Reservoir Simulation

5.3.1 Introduction

Searching for oil and gas is an inherently expensive activity and the need for predicting the performance of a petroleum reservoir is therefore of a great economical advantage. Reservoir simulation has shown to be a prominent method to assessing different production strategies[48]. This is enhanced by the fact that the simulation methods and techniques used are becoming more and more reliable. This section discusses the different aspects of reservoir simulation in addition to its corresponding numerical approaches that are used in the industry. Unless mentioned otherwise, most of the description in the Subsection 5.3.2 is taken from a paper published by Da Silva et al.[32].

5.3.2 Review of Numerical Approaches and Approximation Models

Numerical simulation of the flow in a well is typically based on the standard set of conservation laws in fluid dynamics (Section 4.3). Hence, the basis of the simulation is a system of coupled nonlinear partial differential equations. The common practice is to simulate the flow in the well in only one dimension using averaged values of enthalpy, pressure, and mass flow rates in the cross sectional area of the flow. The components of the flow are usually water in addition to two phases of hydrocarbon pseudo components in standard conditions, oil and gas. The reason behind using pseudo components is to reduce the computational effort by lumping several individual components into few pseudo components. The lumping is based on the components' chemical and physical properties such as boiling point and viscosity for instance[49]. The pseudo components are usually constructed functions of pressure and temperature.

The three traditional hydrocarbon models used in the industry from the simplest to the more complex are the black oil model, the volatile oil model and the fully compositional model. The black oil model assumes that gas can dissolve in oil but not the other way around, whereas in the volatile oil model, the oil and gas pseudo components can be found in both liquid and gas phase. Last, the fully compositional model is based on tracking the mass flow rate of each individual hydrocarbon. Obviously, the latter model is time consuming and is therefore an uncommon approach to flow simulation in a well. It is worth mentioning that all the three hydrocarbon models are used to describe flow in both reservoir and well.

Furthermore, the equations governing the flow in a reservoir are semi-discretized using finite volume methods. The number of grid cells can be in the range of 10^4 to 10^6. The idea behind semi-discretization is that a PDE is discretized in space only while time remains continuous. As a consequence, nonlinear PDE can be approximated with a high dimentional nonlinear ODE[50]. The advantage of this approach is that ordinary ODE solver software can be used to simulate the system efficiently. This is due to their well established routines for error and step-size control.

When it comes to the temporal discretization, both explicit and implicit methods such as backward Euler scheme and fully Newton-Raphson are used. In certain cases, using a combination of implicit and explicit method can be beneficial. The latter approach is used in the so-called IMPES method where the pressure and saturation equations are given an explicit and implicit treatment, respectively[51]. However, the simplest simulation models are based on equidistant explicit finite difference method, while the most advanced models use adaptive step size control (self-adjusting approach). The latter is the most common approach and is based on higher order Runge Kutta methods. Adaptive time stepping scheme decreases the time step if the solution does not converge within a predefined convergence criteria upon using Newton-Raphson procedure. In the other way around, the time step size is increased if convergence occurs way ahead of the predefined maximum number of iterations.

Chapter 6

Reservoir Simulation

In this chapter, simulations of oil recovery from a reservoir based on multirate approach are presented and discussed. The simulations are carried out in Brilliant, which is a software developed by Petrell AS. It should be noticed that the results and the discussions presented in this chapter is only valid for the specific cases related to this study.

6.1 System Characteristics

In this section, the theories from Chapters 2 and 3 are used to discuss the choices taken in regard to the simulations presented in this chapter.

The qualitative analysis discussed in Subsection 5.2.2 proposes four different time constants for the variables in a well-reservoir system. However, for simplification reasons, only two time intervals are used to differentiate between the fast and slow subsystems, i.e. the well and the reservoir, respectively.

Since reservoir simulations are usually costly considering the large number of control volumes that are used in the simulations for long periods of time, i.e. months or years, an implicit approach based on first order upwind method in time is used here. This is in order to be able to use large time steps without facing stability constraints (Appendix B). For the space discretization, the accuracy is of first and second order for the first and second derivative parts in the equations, respectively. In addition, and due to the same reasoning (large amount of data to be stored), the step-skipping approach (Section 2.3.3) is used to couple the well and the reservoir subsystem together. In practice, this is done by deactivating the well subsystem to allow for larger time steps in the reservoir subsystem. Hence, the value of each variable in the well subsystem is assumed to be constant and not updated (skipped) until the well subsystem is activated again. There are two criteria

for deactivating the well subsystem in this study, one is based on time and the other on pressure. Both criteria are explained in more detail in Sections 6.5 and 6.6.

When the well subsystem is activated, the entire system becomes bounded by the time step dictated by the stability in the well subsystem. Although the well subsystem is simulated using an implicit method, the subsystem can still encounter instability induced by coupling equations that are solved iteratively. One example of such case is solving the Navier-Stokes equation using the SIMPLEC approach. On the contrary, the equations that govern the flow in the reservoir subsystem are solved without the need of iteration, hence, no stability issues are presented. In addition, and taking into consideration that the flow velocity in the reservoir is much lower than in the well, the time step in the reservoir subsystem is allowed to be much larger than the well subsystem without sacrificing accuracy.

6.1.1 Multirate Approach in Reservoir Simulation

Using the step skipping-approach entails running the entire system with the same time step simultaneously, which in turn means that the communication between the subsystems is monolithic (Section 2.1). As the interactions between the two subsystems take place on the same time scale (using the same time step) and in multiple ways (discussed in Section 5.2.2), the coupling between the two subsystems can be classified as strong (see Section 2.2). In addition, both subsystems influence each other at the boundary between the well and the reservoir, where information about pressure, temperature and mass flow are exchanged. Hence, a fully-dynamic coupling is suitable for this case (Section 2.3). Taking into consideration that the subsystems interact with each other through their governing equations, the coupling between the physics in the well and the reservoir is said to be volumetric (Section 2.2).

Furthermore, each of the two subsystems are described with different field equations in which the variables in each field can be a function of the variables of the other field. Therefore, the well-reservoir system is considered to be a coupled multi-field problem (2.2). Last, as the pressure in the reservoir gradually approaches the pressure in the well throughout the simulation time, the time constants of the two subsystems also change as a consequence. Hence, the most suitable approach for determining the rate of change in each subsystem is to use a self-adjusting method (Section 3.6). In other words, no predefined time step must be given based on R_c in this case since R_c is not a constant. As a reminder, R_c is defined as the ratio of the time constant in slow subsystem to its corresponding value

in the fast subsystem (Section 3.1). An overview of the six characteristics of a multirate approach related to the well-reservoir system in this study is given in the list below (reference to Table 3.1):

- Strength of coupling: Strong.
- Coupling strategy: Step-Skipping approach.
- Coupling between physics: Volumetric.
- Coupling problem: Coupled multi-field.
- Time constant analysis: Self adjusting approach.
- Multirate philosophy: Monolithic.

6.1.2 Calculation Sequence in Brilliant

The equations governing the well-reservoir dynamics (Chapter 4) are solved in a specific order, or sequence, in Brilliant as shown in Table 6.1. The convergence test in the fifth step in the reservoir subsystem checks whether or not mass is conserved. If not, the process is sent back to start from the pressure equation.

Table 6.1: Calculation sequence in each subsystem starting from the top and moving downwards.

Reservoir subsystem	Well subsystem
Pressure	Velocity, pressure and density (SIMPLEC solver)
Pressure gradient	Enthalpy and mass fraction
Darcy velocity	Density
Check for convergence	
Enthalpy and mass fraction	
Density	

Thermodynamic data of the hydrocarbons used in this study are integrated in the software, hence no manual input of data is needed. Fluids are assumed to be compressible by default in Brilliant, hence density must be calculated. Density calculation in both subsystems is based on the pressure and enthalpy of the fluid using Peng and Robinson equation of state[52].

6.2 Geometry, Setup and Preliminary Analysis

As discussed earlier, well-reservoir dynamics is three dimensional in nature and must therefore be modelled accordingly. With reference to Section 6.3.2, the velocity in the well is shown to be much higher than in the reservoir. Hence, the accuracy of the solution in the well becomes much lower compared to the reservoir if the same temporal and spatial steps are used for both subsystems. Therefore, the control volumes in the reservoir are allowed to be larger compared to those of the well subsystem and the region around as shown in Fig. 6.1, where the gradients are larger than the region further away from the well.

The well configuration used in the simulations is vertical (see Appendix A.2) and the effects of gravity is neglected for simplification reasons. This leads to a bilaterally symmetric reservoir that can be divided into equal mirror halves[61]. Such property is utilized such that only one-half of the reservoir is simulated as shown in Fig. 6.1, which in turn leads to a significant reduction in the overall simulation time.

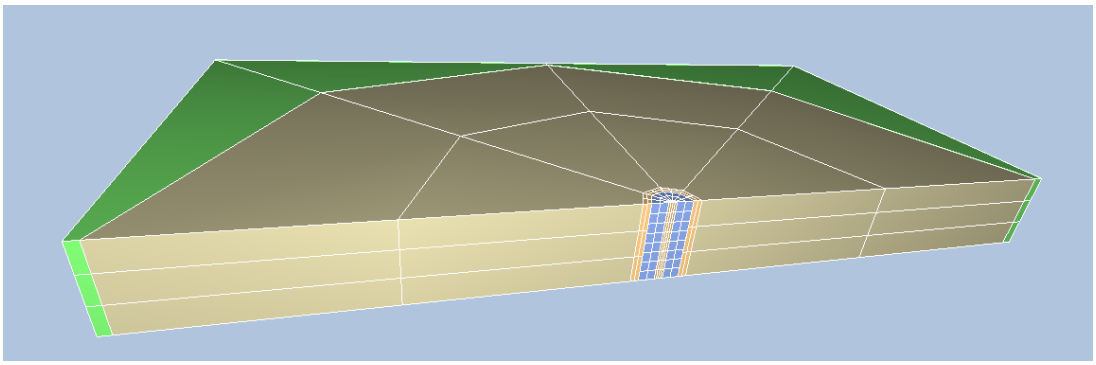

Figure 6.1: The geometry of the entire reservoir with the well in the centre of the reservoir. The different colors in the figure is not of importance here.

The main hydrocarbon used in the simulations is n-pentane (referred to as pentane hereafter). However, since the effects of deactivating the well subsystem is of concern in this study, n-hexane is introduced in a region forming a ring around the well (referred to as hexane hereafter), see the right hand side of Fig. 6.2. Hexane is used as a species to trace the flow of the hydrocarbons into the well. Most importantly, the amount of both hexane and pentane flowing in the well is studied here to measure the effects of deactivating the well subsystem. The left hand side of Fig. 6.2 illustrates the top and bottom side of the well along with the direction of the flow. The pressure at the outflow, which lies at the tip of the red arrow at the top side, is used as a variable to lower the pressure in the well, which in turn leads to the flow of the hydrocarbons into the well. In other words, the

boundary conditions in the well at the top and bottom side are Neumann and Dirichlet boundaries, respectively, where the velocity vector at the Dirichlet boundary is equal to zero[66]. Hence, the flow from the reservoir can only exit the system through the outflow at the top side.

The origo of the coordinate system is placed at the bottom centre of the well such that the positive z axis indicates the direction of the flow upwards. The x-y plane lies perpendicularly to the well, i.e. the normal of the x-y plane is parallel to the z axis. The cross sectional area of the reservoir (x-y plane) is a square with an area of $1\,\mathrm{km}^2$ and the radius of the well is 0.05 m. The inner and outer radius of the region containing hexane measured from the centre of the well is 5 m and 25 m, respectively. The length of the well and the permeability of the reservoir are the two variables that are changed throughout this study, while all the other variables remain constant.

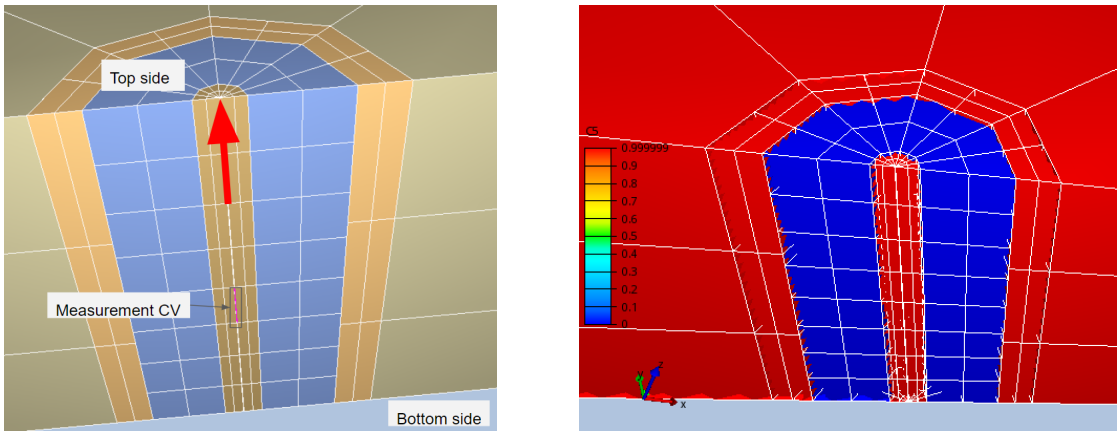

Figure 6.2: Left: Region around the well. The red arrow indicates the direction of the flow in the well. Right: Distribution of pentane (C5) and hexane in the reservoir. The red and blue colors mark the region containing pentane and hexane, respectively.

For simplification reasons, both pressure and temperature are considered to be uniform initially along the depth and throughout the reservoir. In addition, the type of reservoir chosen here is homogeneous and isotropic (see Appendix C). The initial temperature and pressure in both the reservoir and the well are chosen to be 110°C and 300 bar, respectively. The outlet pressure is then dropped from 300 bar to 250 bar during a period of 500 s to initiate the flow into the well. In order to maintain the simulations as simple as possible, the hydrocarbons must remain in one phase throughout the entire simulation time period, which is liquid in this case. Both pentane and hexane remain in liquid phase according to their phase diagrams despite the pressure drop to 250 bar. Temperature changes throughout the simulations presented here are small and are therefore not anal-

ysed further in this study. Considering that the temperature changes are insignificant and that the C_p value of both pentane and hexane er relatively close to each other (throughout simulation), the assumption of almost constant C_p mentioned in Subsection 4.2.3 is therefore justified.

All the measurements in the well, unless other is specified, are taken in a control volume in the middle of the domain. This control volume is referred to as "Measurement CV" in Fig. 6.2. The reason behind this is that since the geometry, pressure, temperature and the distribution of the hydrocarbons are symmetrical around and along the depth of the well, measurements in the middle of the well are assumed to represent the average conditions in the entire well.

6.3 Verification and Validation

A simulation software, like any other software, would only give results based on the input data provided by the user without carrying out a logic test. The only logic in the way a software should behave comes from the user. Therefore, it is important to check whether or not the software solves the problem in hand in a correct manner. To do so, the results produced by the software should be both validated and verified. Validation is the process of determining the match between the numerical results to those of real world measurements to quantify the deviation. Verification, on the other hand, is the process of determining that a model implementation accurately represents the developer's conceptual description of the model[53]. Since the combination of the dimensions and the variables used in this study is unique, the attempt for validating the results is not feasible. However, the simulation results can still be verified by investigating whether or not they are physical, which is the matter of discussion in this section.

6.3.1 Pressure

As mentioned earlier, the pressure at the well outlet is reduced from 300 bar to 250 bar in 500 s. Since the pressure in the fluids inside the well is propagated with the speed of sound[54], the pressure in the entire well remains close to 250 bar after 500 s, while the pressure around the well remains relatively high as shown in Fig. 6.3. This, in turn, leads to the flow of hydrocarbons from the reservoir into the well. The rate of the flow is the highest at 500 s since the pressure difference between the well and the reservoir then is the highest, as shown to the right of Fig. 6.17. Throughout passage of time, the pressure difference becomes smaller leading to a lower recovery rate of the hydrocarbons in the

reservoir. Furthermore, the gradient of the pressure in the reservoir increases towards the well as shown in Fig. 6.4. This is to be expected from the discussion in Section 5.1.

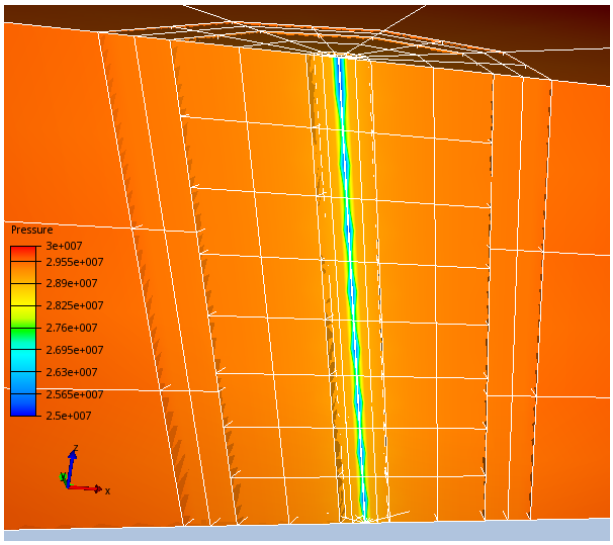

Figure 6.3: Pressure profile after 5000 s into simulation measured in Pascal.

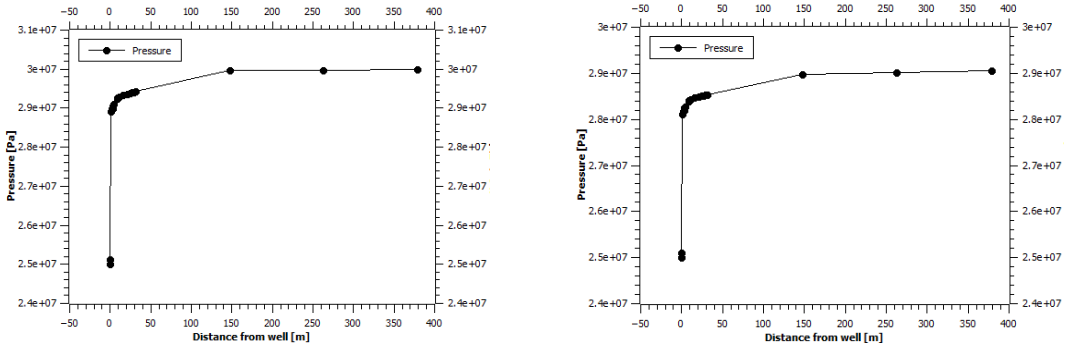

Figure 6.4: Left: Pressure vs. distance from the well after 10^3 s. Right: Pressure vs. distance from the well after 10^5 s.

6.3.2 Velocity

While the well is in production, it is expected that the hydrocarbons in the reservoir flow into the well from all directions continuously, and that the velocity becomes higher closer to the well (due to higher pressure gradient). At the same time, the flow velocity in the well in the z direction is expected to be at its highest close to the outlet, while declining towards zero at the bottom side of the well. These two expectations are confirmed in the simulation as shown in Fig. 6.5

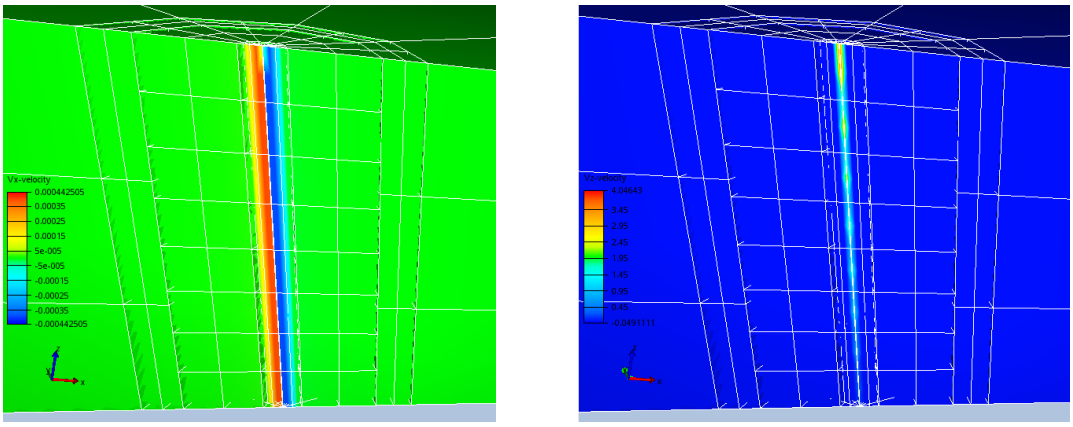

Figure 6.5: Left: x-component of the flow velocity in the reservoir. Right: z-component of the flow velocity in the well. Both figures are taken after 5000 s into simulation. The velocities are measured in m/s.

Notice that the highest velocity in both the reservoir and the well according to Fig. 6.5 are 0.0004 m/s and 4 m/s, respectively. In other words, the flow in the well is approximately 10^4 times faster than the flow in the reservoir. Since velocity is the key variable for transporting energy, species and momentum in the well-reservoir system, variables in a subsystem with high velocity experience rapid changes as a consequence. Therefore, the well subsystem is defined as the fast subsystem compared to the reservoir subsystem.

6.3.3 Intermediate Conclusion

The simulation results from the inspection of the pressure and velocity profiles suggest that the well-reservoir model functions as expected in Brilliant. In other words, it can be said that the model is verified. The next step is to deactivate the well subsystem and trace the amount of the hydrocarbons entering and exiting the well, which in turn yields an estimation of the error induced by the deactivation.

6.4 Error Estimation

The mass fraction of pentane in the Measurement CV, see Fig. 6.11, is used as basis for error estimation when the well subsystem is deactivated (multirate approach used). The reason for this is to study the effects of the deactivation on the transport of species in the well-reservoir system. The idea is to compare the results with the case where the entire system is run without deactivation (single-rate). The mass fraction of pentane calculated using multirate and single-rate approaches are referred to as $C5_{multirate}$ and $C5_{single-rate}$, respectively. The error is measured as a relative error, or RE in short, using the following equation

$$Relative\ Error = \left| \frac{C5_{single-rate} - C5_{multirate}}{C5_{single-rate}} \right|. \tag{6.1}$$

It is worth mentioning that Eq.(6.1) is chosen due to its simplicity, i.e. other types of error estimators can also be used. An example of a simulation run using both multirate and single-rate approaches is illustrated in Fig. 6.6. The figure shows that the mass fraction of pentane changes much faster in the first $2 \cdot 10^5$ s compared to the following time period. The region with fast changing mass fraction is referred to as the dynamic region in this study. It is the dynamic region that is of importance here since the error is anticipated to be higher compared to the regions where changes occur over longer periods of time. Note that the dynamic region is unique to each case depending on the well length and the permeability of the reservoir.

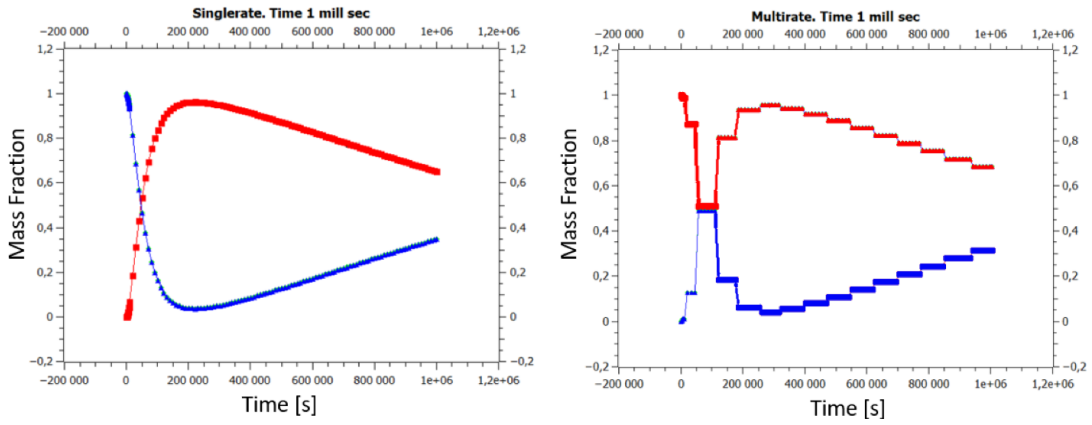

Figure 6.6: Mass fraction of pentane (blue) and hexane (red) measured in the Measurement CV. Single-rate and multirate approaches are used in the figure to the left and right, respectively.

6.5 Time Based Deactivation

The time based deactivation approach relies on a predefined period of time (defined by the user) to keep the well subsystem both activated and deactivated. The period in which the well subsystem remains active is chosen to be 600 s to allow the content of the well to be flushed out at least once. This ensures that the well subsystem is updated with the conditions in the reservoir each time the well subsystem is activated. Looking at Fig. 6.7, it is obvious that the velocity in the well is linearly increasing from the bottom to the top of the well. This is due to the gap between the lines being equidistant. Hence, using the velocity given by the red line (average velocity), i.e. 2 m/s in case of having a permeability

of $10^{-13}\,\mathrm{m}^2$, the time it takes for fluids to be completely transported out from the bottom to the top of a 100 m long well is 50 s. Different cases were tested in regard to this study using different well lengths and reservoir permeabilities. The results in each case was the same, which is, the velocity profile in the well is always linear (with different average values). Therefore, using the values measured in the Measurement CV is regarded as a sufficient approximation for the average conditions in the well. Moreover, the reason behind choosing a standard activation time of 600 s is to ensure that the content of the well is flushed out at least once in all the cases that are presented in this section.

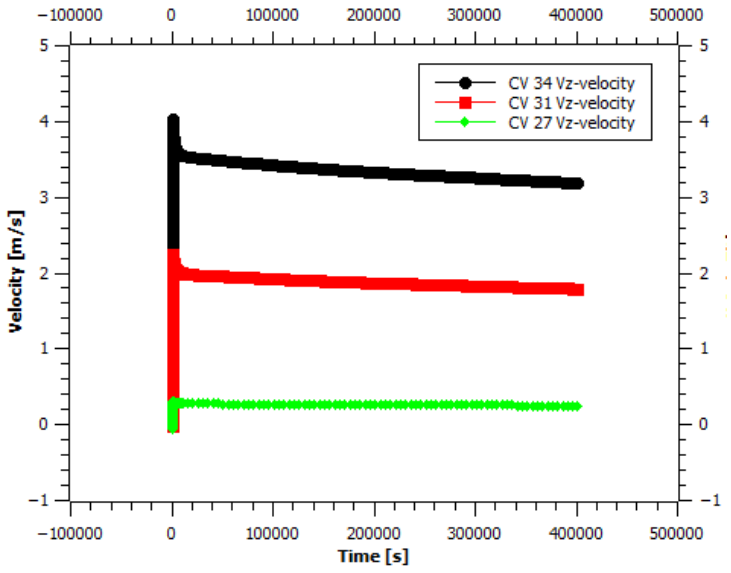

Figure 6.7: Velocity profiles in the well in the z direction throughout simulation time. The green, red and black lines refer to measurements taken in the bottom, middle and top regions of the well. The permeability and the length of the well used here are $10^{-13}\,\mathrm{m}^2$ and 100 m, respectively.

The deactivation time, on the other hand, is used as a variable to measure the error propagation induced by using multirate approach. Dividing deactivation tiime on activation time yields the deactivation ratio, see Eq.(6.2). When the well subsystem is deactivated for a period of 1200 s, for instance, the deactivation ratio is said to be two relative to the activation period, which is set to 600 s. The deactivation ratio ranges from one to five in this study ([1:1:5]).

$$Deactivation\ Ratio = \frac{Deactivation\ time}{Activation\ time} \tag{6.2}$$

6.5.1 Results of Varying Length and Permeability

Using a 100 m long well and $\kappa = 10^{-13}\,\mathrm{m}^2$, the maximum relative error (Eq.(6.1)) measured in the case of using deactivation ratios of 5 and 1 are 7% and 1.5%, respectively, as shown to the right in Figs. 6.8 and 6.9. The relative error is referred to as RE hereafter. The measurement frequency used in the figures is one sample per 5000 s. The effect of the activation and deactivation of the well subsystem can be seen in the fluctuations in the RE profiles to the right of Figs. 6.8 and 6.9.

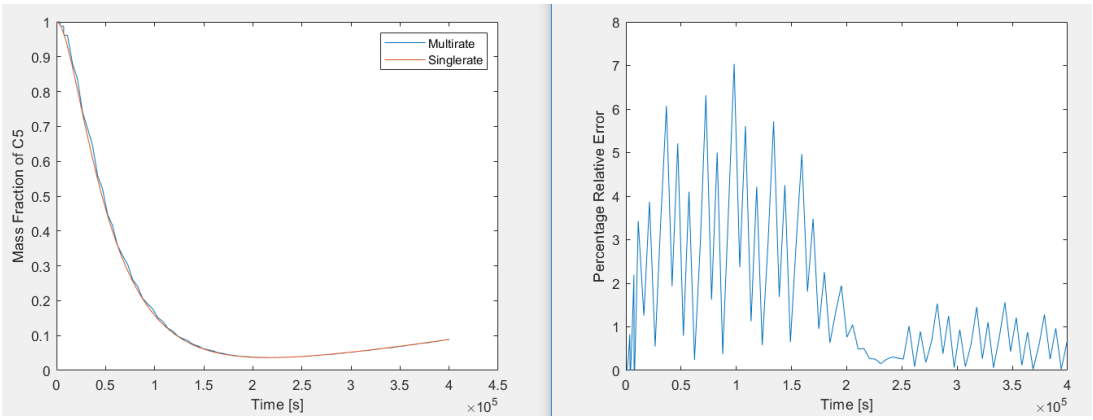

Figure 6.8: Deactivation ratio = 5 (deactivation period of 3000 s). Left: Mass fraction of pentane using multirate and single-rate approaches. Right: RE given in percentage.

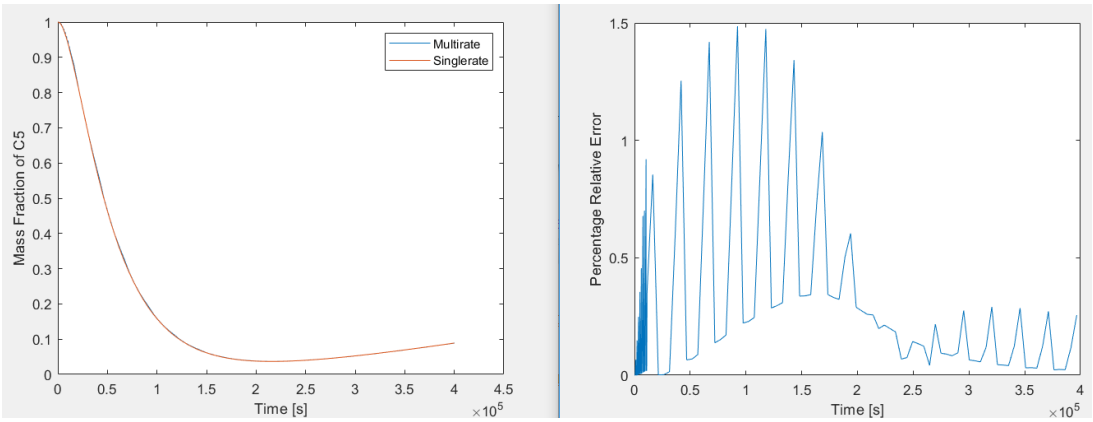

Figure 6.9: Deactivation ratio = 1 (deactivation period of 600 s). Left: Mass fraction of pentane using multirate and single-rate approaches. Right: RE given in percentage.

Using a high sampling frequency such as in Fig. 6.10, the effect of deactivation can be seen clearly. When the well subsystem is deactivated, all the variables in the well, including the mass fraction of pentane, are held constant throughout the deactivation time. This can be seen in Fig. 6.10, where the mass fraction is horizontal for 3000 s when using a deactivation ratio of 5.

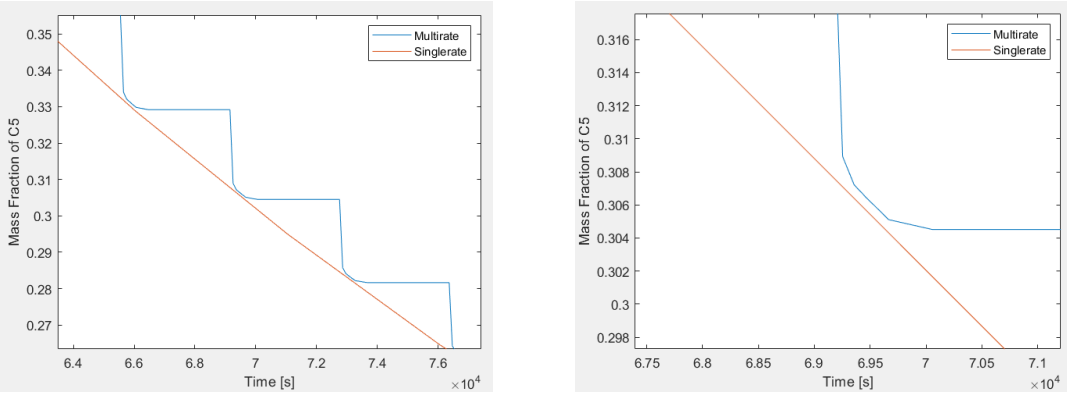

Figure 6.10: Plot from Fig. 6.8 using high sampling frequency. Left: Zoomed plot. Right: Extra zoomed plot.

Likewise, 15 cases are investigated initially using a 100 m long well against three permeabilities and five deactivation ratios ranging from one to five ($3 \cdot 5 = 15$). The maximum RE for each case is presented in Table 6.2 and plotted in Fig. 6.12.

Table 6.2: Maximum RE in percentage using 100 m long well.

	Deactivation ratio				
Permeability $[m^2]$	1	2	3	4	5
10^{-14}	0.17	0.33	0.49	0.62	0.8
$5 \cdot 10^{-14}$	0.78	1.4	2.2	2.8	3.5
10^{-13}	1.5	2.75	4.2	5.6	7

The trend shows that the lower the permeability, the lower is the RE. This is expected as the permeability is proportional to the velocity in the reservoir according to Eq.(4.3). Having low velocity entails that the condition in the reservoir change at a slow pace (less transport of pentane). The Measurement CV is fed by fluids from the reservoir around and the stream in the well from below as shown in Fig. 6.11. Therefore, a slow changing reservoir condition induces lower error as less information is lost to a deactivated well subsystem.

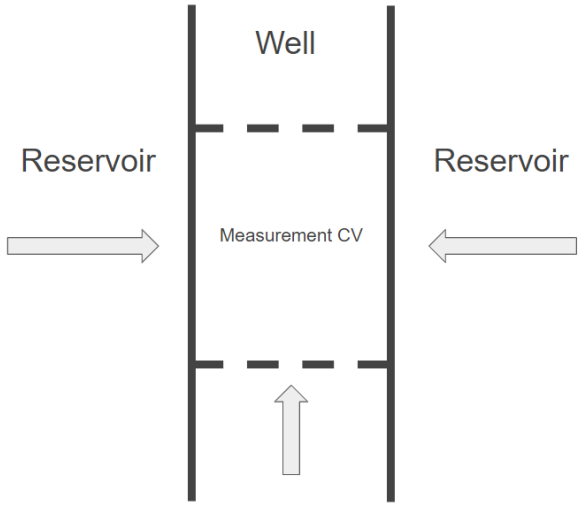

Figure 6.11: Illustration of the Measurement CV.

The results from Fig. 6.12 show that the maximum RE for each permeability value increases linearly with the deactivation ratio as the gradient of the curves are almost constant. In a similar way, the maximum RE for each deactivation ratio increases linearly with the permeability as well. The reason behind the latter trend is that when all the other variables are kept constant, the permeability becomes linearly proportional to the velocity in the reservoir according to Eq.(4.3).

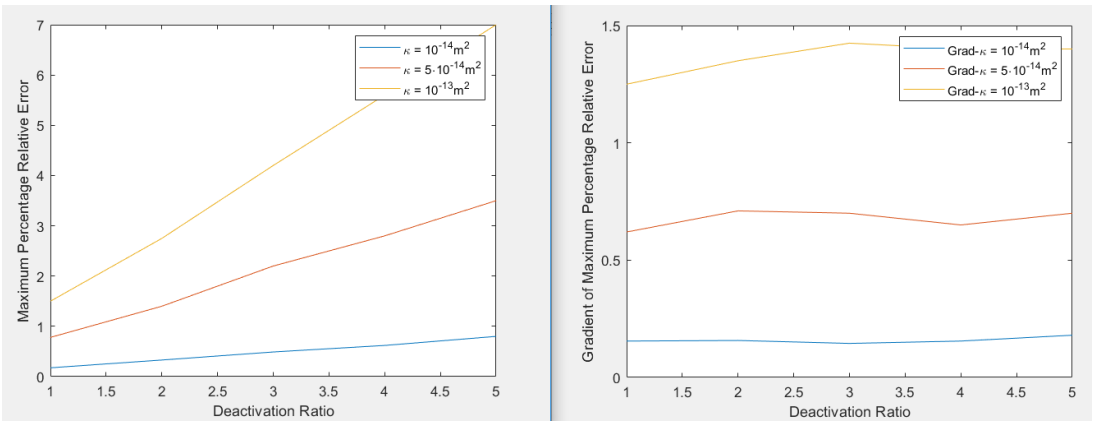

Figure 6.12: Left: Plot of the values from Table 6.2. Right: Gradient of the three curves related to each permeability from the figure to the left.

Further tests were conducted using well lengths of 50 m and 200 m against the same three permeability values. The maximum RE measured in the case of deactivation ratio of 5 and well length equal to 200 m is 7%. While in case of using a deactivation ratio of 1 and well length equal to 50 m, the maximum RE is shown to be 1.5%, see Fig. 6.13. Although not each case was tested one by one, the trend is however clear. Varying the length of the well yields almost the same maximum RE when plotted against the five deactivation

ratios. The RE profiles of the results obtained using the lengths 50 m and 200 m differ slightly from the one using 100 m. In other words, the maximum RE is a function of only the permeability and not the length of the well in these cases. The reason behind this is that the pressure in the well increases slightly along the depth, see to the right of Fig. 6.18, such that it remains almost uniform when using the lengths 50 m, 100 m and 200 m. Keeping the permeability constant, the velocity in the reservoir is only affected by the pressure gradient according to Eq.(4.3). Hence, the flow of information from the reservoir into the Measurement CV remains almost the same when using short well lengths such as 50 m,100 m and 200m.

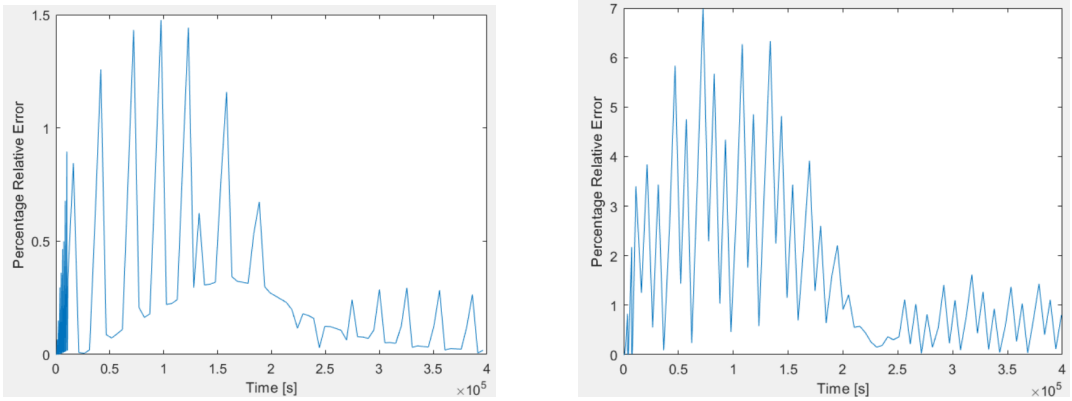

Figure 6.13: Left: The length of the well is 50 m and the deactivation ratio is 1. Right: The length of the well is 200 m and the deactivation ratio is 5. The permeability used here is $\kappa = 10^{-13}\,\mathrm{m}^2$.

It is worth mentioning that the results obtained by varying the length are restricted to the geometry and the distribution of hydrocarbons used here, which is symmetrical along the depth of the reservoir. Put it differently, in case of having an unsymmetrical distribution of hydrocarbons along the depth, the flow of fluids into the Measurement CV from below (the well) would defer depending on the length. This is due to the fact that different hydrocarbons can be present along the depth, which in turn would affect the mixture of hydrocarbons measured in the Measurement CV. In such a case, the profile of RE could be significantly different than the ones measured in this study.

Relative Error Profile

The plots of RE used in this study are in absolute form, i.e. always positive as shown in Eq.(6.1). However, by omitting the absolute sign and plotting the case in Fig. 6.8 again, see to the right of Fig. 6.14, the sign of the RE changes around $2.3 \cdot 10^5$ s. The

reason for this is that the derivative of the mass fraction also changes sign at that point. Furthermore, the value of the mass fraction calculated using multirate approach is always higher than its corresponding value using single-rate approach until around $2.3 \cdot 10^5$ s as shown in Fig. 6.14. Since the profile of the mass fraction using both approaches cross each other at that point, they must come closer and closer to each other prior to reaching the point. This is the reason behind the reduction of the absolute value of RE after reaching a top at around 10^5 s in Figs. 6.8 and 6.9. The absolute value of the first derivative of the mass fraction is very low after the crossing point compared to the period before as shown to the left of Fig. 6.14. This is why the RE remains low in the period after the crossing point (around $2.3 \cdot 10^5$ s).

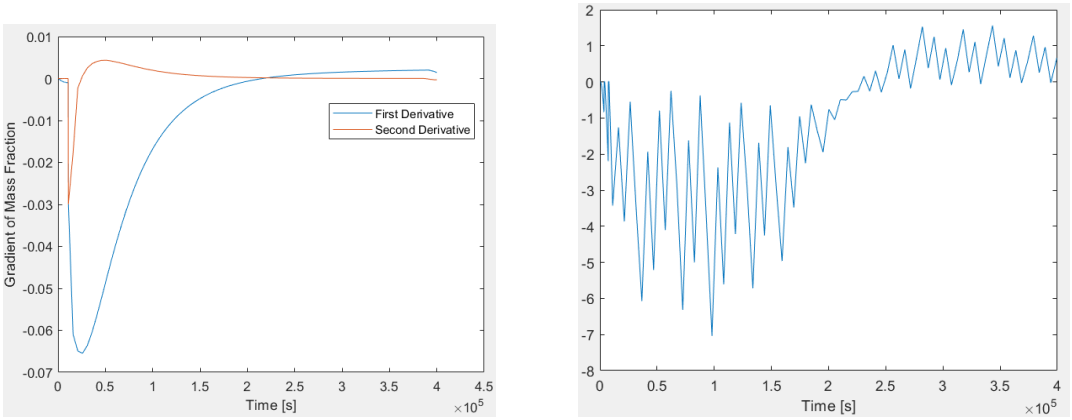

Figure 6.14: Left: First and seconds derivatives of the mass fraction of pentane using single-rate approach from the case in Fig. 6.8. Right: The vertical axis represents percentage relative deviation from Fig. 6.8.

Time Scale of the Reservoir Subsystem

Looking to the left of Fig. 6.8, it can be seen that the lowest mass fraction of pentane is measured at around $2 \cdot 10^5$ s when using $\kappa = 10^{-13}\,\mathrm{m}^2$. On the other hand, and when using $\kappa = 10^{-14}\,\mathrm{m}^2$, which is 10 times lower than the former permeability, the lowest mass fraction is measured at around $2 \cdot 10^6$ s, see Fig. 6.15, which is 10 times higher than in case of $\kappa = 10^{-13}\,\mathrm{m}^2$. The time constant of the two cases, i.e. 63% of the time it takes to reach the lowest mass fraction, are measured to be $38,000s$ and $380,000s$ when using $\kappa = 10^{-13}\,\mathrm{m}^2$ and $\kappa = 10^{-14}\,\mathrm{m}^2$, respectively. This leads to the conclusion that the time scale of the reservoir subsystem is linearly proportional to the permeability in the reservoir. The effects of the well length is negligible in regard to the time scale as the profile of the mass fraction remains almost the same for the lengths 50 m, 100 m and 200 m as observed in the simulations.

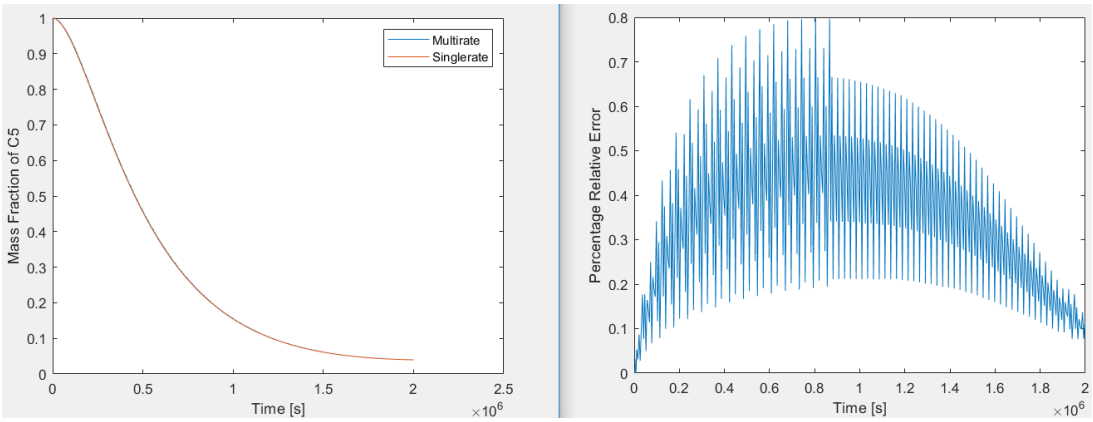

Figure 6.15: Low-permeability reservoir with a deactivation ratio of 5. The permeability and the well length are $\kappa = 10^{-14}\,\mathrm{m}^2$ and 100 m, respectively.

6.5.2 Sampling in Reservoir

As shown in the previous figures such as in Figs. 6.8 and 6.9, the absolute RE profiles are always above zero in the dynamic region before converging towards zero. The reason behind the convergence , as discuessed earlier, is that the gradient of the mass fraction of pentane becomes sufficiently small, which in turn allows the multirate approach to almost align with the results obtained by the single-rate approach. However, in an attempt to explore the reason behind why the RE is never zero in the dynamic region, a closer look was taken into the conditions in the reservoir rather than focusing on the Measurement CV, which is located in the well. This time, the same measurements are taken in a control volume located four meters away from the Measurement CV at different depths, see Fig. 6.16. The length of the well and the permeability used in this case are 100 m and $10^{-14}\,\mathrm{m}^2$, respectively.

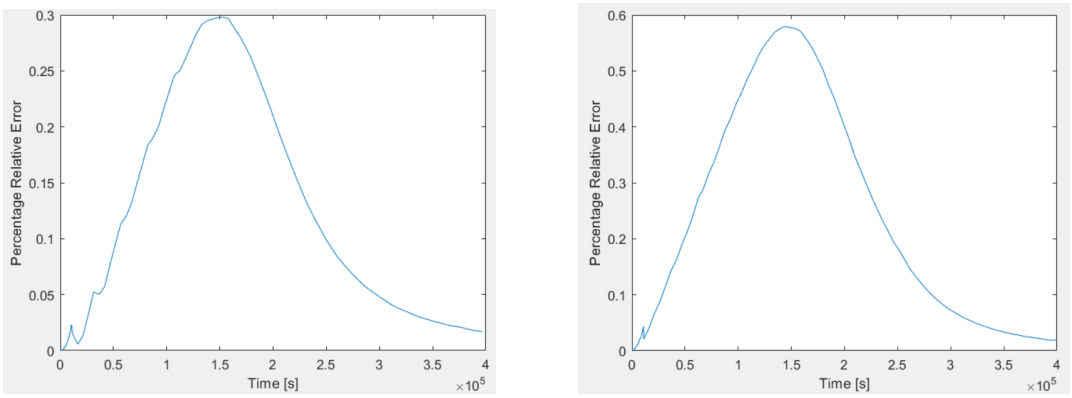

Figure 6.16: Left: Deactivation ratio = 1. Right: Deactivation ratio = 5. Both samples are taken at $z = 50\,\mathrm{m}$.

Results from the measurements taken at different depths align almost perfectly with the

ones taken at a depth of 50 m as in Fig. 6.16 for different deactivation ratios. For instance, the same RE profile is obtained using a deactivation ratio of 5 at different depths. This is due the fact that the pressure in the well is almost uniform as discussed in Section 6.5, hence, the reservoir conditions becomes almost uniform along the depth as a result.

Moreover, the results show that the profile of RE is always above zero in the reservoir even though the reservoir subsystem is never deactivated. This leads to the conclusion that the reservoir subsystem is influenced by the deactivation of the well subsystem. The reason for this is that when the well subsystem is deactivated, the pressure in the well remains constant throughout the deactivation time. The pressure difference between the well and the reservoir, on the other hand, influence the velocity of the flow in the reservoir near the well as discussed earlier. Furthermore, velocity changes near the well affects the velocity in the entire reservoir due to mass conservation, which in turn also affects the pressure in the entire reservoir. In other words, by deactivating the well subsystem one accepts that the entire system is altered permanently. This is also shown to the right of Fig. 6.10 where the profile of mass fraction using multirate approach becomes parallel to the one using single-rate approach. At this point, and from a multirate point of view, the well subsystem is completely updated with the reservoir subsystem. However, since the conditions in the reservoir are also changed due to the deactivation process, there will always be a minimum error in the system represented by the gab between the two parallel lines (for instance at around $6.95 \cdot 10^4$ s in Fig. 6.10). The only question that remains to ask is how large maximum RE the user is willing to accept, which in turn can be controlled by the deactivation ratio. Moreover, the fact that the deactivation of the well subsystem influence the conditions in the reservoir subsystem is an evidence of that the two subsystem are strongly coupled.

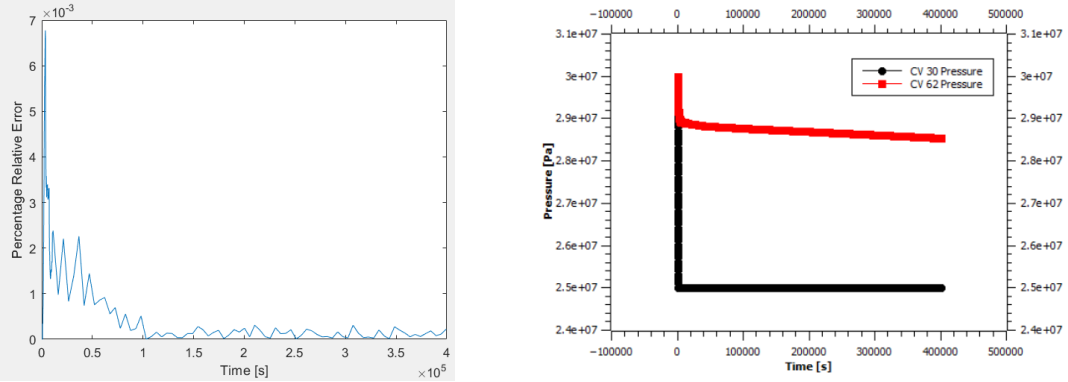

Figure 6.17: Left: RE of using multirate approach with deactivation ratio of 5 measured in the reservoir using pressure instead of mass fraction of pentane. Right: Pressure profiles in the well and the reservoir at the interface. The red and black lines refer to the pressure in the reservoir and the well, respectively. The permeability is $10^{-13}\,\mathrm{m}^2$ and the length of the well is 100 m.

Further tests were conducted to ensure that the hypothesis of the reservoir subsystem being affected by the deactivation of the well subsystem is correct. This time, the basis for RE calculation in Eq. (6.1) is pressure instead of mass fraction of pentane. The result of the sampling taken near the well, i.e. left to Fig. 6.17, shows that RE is always above zero. Hence, the hypothesis is strengthened even further. Moreover, the pressure plot in the reservoir and the well at the interface in between is illustrated to the right of Fig. 6.17. The difference between the two lines (pressure gradient) is the main driver of the flow into the well.

Deactivating the well subsystem for a predefined period of time (deactivation time) requires experience and knowledge about the geometry and distribution of the hydrocarbons in the reservoir. For instance, knowing that the permeability is low allows for increasing the deactivation time for the same maximum RE. Although the method is easy to implement and gives the user full control over the deactivation process, it does not account for the dynamics in the system automatically. To do so, a different deactivation approach is tested in Section 6.6 based on pressure changes both in the reservoir and the well.

6.6 Pressure Based Deactivation

The pressure based deactivation approach enables automatic deactivation of the well subsystem when the gradient of the pressure in the Measurement CV (in the well), $\partial p/\partial t$, is beneath a predefined threshold, or a deactivation criterion. Looking to the right of Fig. 6.18, it is obvious that the gradient of the pressure remains stable at around 0.001 Pa/s for

long period of time. The deactivation criterion must therefore be higher than 0.001 Pa/s or the well subsystem would never be deactivated otherwise. At the same time, it must be chosen such that the well subsystem can be deactivated rapidly in order to reduce the overall simulation time. Hence, the deactivation criterion must be much higher than 0.001 Pa/s. After a few trials, a deactivation criterion of $\frac{\partial p}{\partial t} = 10\,\text{Pa/s}$ was found to be suitable. On the other hand, and in order to activate the well subsystem again, an activation criterion based on the pressure changes, Δp, at the interface of the Measurement CV must also be predefined. For instance, choosing an activation criterion of $\Delta p = 100\,\text{Pa}$ entails that when the pressure is 100 Pa higher at the interface of the Measurement CV since the last deactivation, the well subsystem becomes activated again. Fig. 6.19 shows the pressure profile and its gradient measured at the interface between the Measurement CV and the reservoir. For each combination of κ and well length L, the simulations are tested for activation criteria ranging from $\Delta p = 100\,\text{Pa}$ to $\Delta p = 500\,\text{Pa}$ with increments of $\Delta p = 100\,\text{Pa}$ ($\Delta p = [100 : 100 : 500]\,\text{Pa}$).

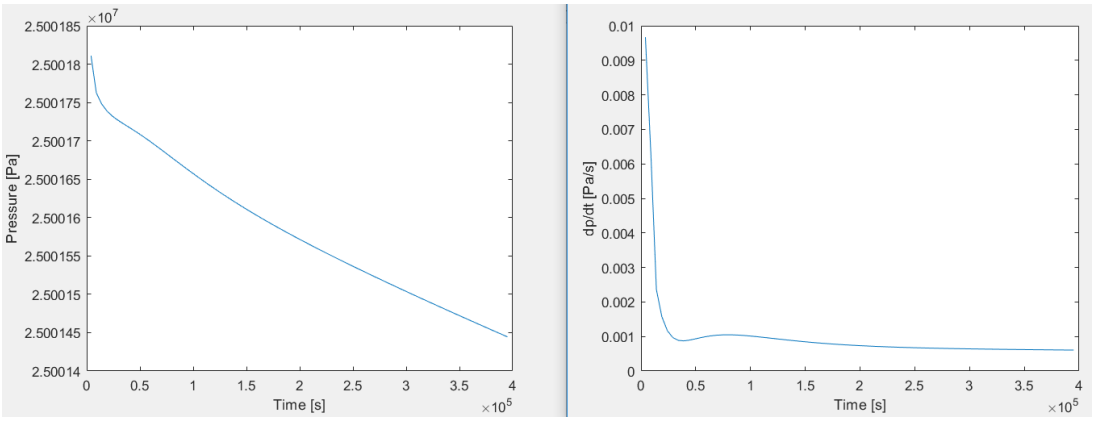

Figure 6.18: Left: Pressure in the Measurement CV. Right: Gradient of the pressure ($\frac{\partial p}{\partial t}$) in the Measurement CV (from the figure to the left). The simulation is carried out using single-rate approach. Sampling starts from 1000 s. The permeability and the length of the well used here are $10^{-13}\,\text{m}^2$ and 50 m, respectively.

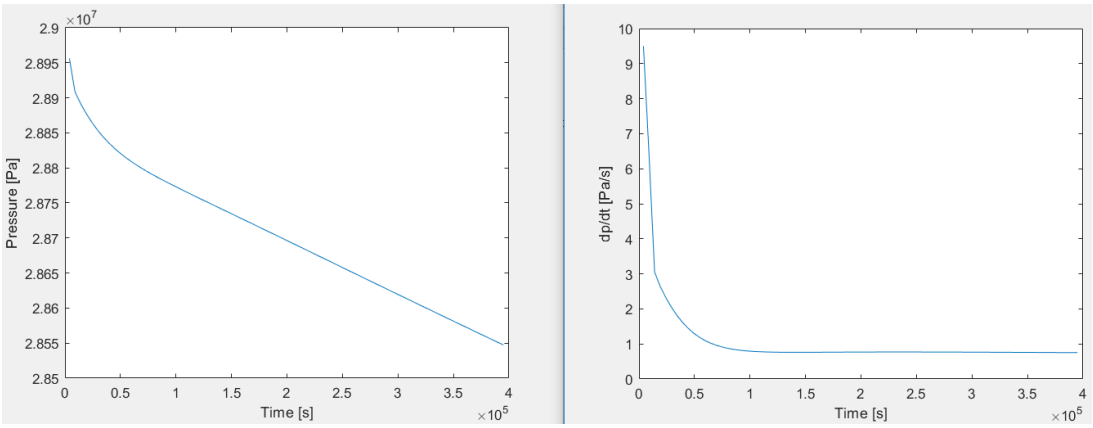

Figure 6.19: Left: Pressure at the interface of the Measurement CV. Right: Gradient of the pressure at the interface of the Measurement CV (from the figure to the left). The simulation is carried out using single-rate approach. Sampling starts from 1000 s. The permeability and the length of the well used here are $10^{-13}\,\mathrm{m}^2$ and 50 m, respectively.

In this section, a total of 25 simulations were carried out using two different well lengths and three permeabilities against five activation criteria (Δp). The maximum RE of each simulation is listed in Table 6.3 and plotted in Fig. 6.20.

Table 6.3: Maximum RE from the simulation results using pressure based deactivation. The length of the well is represented by L.

	Δp [Pa]				
Cases	100	200	300	400	500
$\kappa = 10^{-13}\,\mathrm{m}^2$, $L = 50\,\mathrm{m}$	1.03	1.03	1.7	2.4	3.1
$\kappa = 5 \cdot 10^{-13}\,\mathrm{m}^2$, $L = 50\,\mathrm{m}$	0.42	0.95	1.75	2.2	2.5
$\kappa = 10^{-14}\,\mathrm{m}^2$, $L = 50\,\mathrm{m}$	0.5	0.85	1.0	1.25	1.57
$\kappa = 10^{-14}\,\mathrm{m}^2$, $L = 100\,\mathrm{m}$	0.6	1.15	1.05	1.4	1.7

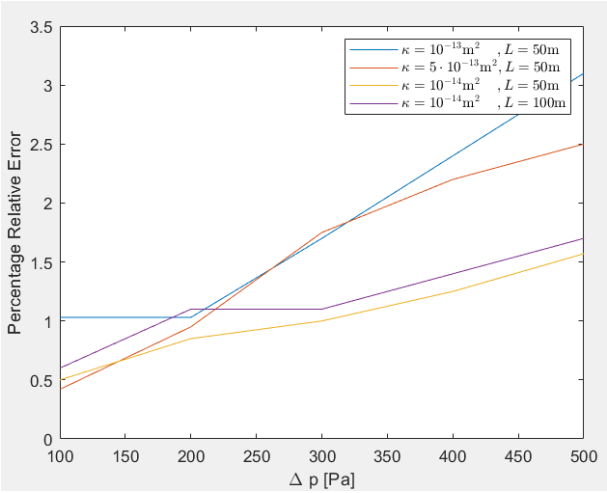

Figure 6.20: Plot of the results from Table 6.3

Looking at the results from Fig. 6.20, three trends can be observed. The first one is that the maximum RE in all the cases tend to be proportional with Δp, which is to be expected as the deactivation period becomes larger with higher Δp (hence larger error). The second is that the lower the permeability, the lower the maximum RE becomes. This is true for all the cases except for the one where $\kappa = 5 \cdot 10^{-13}\,\mathrm{m}^2$ and $L = 50\,\mathrm{m}$ are used. The reason behind the proportionality between the maximum RE and permeability is the same as with the case of using time based deactivation (discussed in Section 6.5). The third trend, which is shown in the case where $\kappa = 10^{-14}\,\mathrm{m}^2$ is used with both $L = 50\,\mathrm{m}$ and $L = 100\,\mathrm{m}$, is that the longer the well length, the higher the maximum RE becomes for all the values of Δp. It should be noticed that these are only trends and do not apply in every case.

The results from Fig. 6.20 show that the maximum RE is a function of both the permeability and the length of the well. These results are different from the cases where time based deactivation are used, which show that the maximum RE is only a function of the permeability (see Section 6.5). To answer the question of why the pressure based deactivation is sensitive to the length of the well, a closer look was taken at one of the simulations such as the one in Fig. 6.21. The figure shows that the lines representing the mass fraction using multirate and single-rate approaches are never aligned in parallel. This means that using the pressure based deactivation approach, the content of the well is never flushed out completely, which in turn means that the well is never fully updated with the conditions in the reservoir. In other words, a sample of a species travelling in the bottom of the well experiences several deactivations of the well subsystem before reaching the top of the well. Hence, the longer the travelling distance (length of the well), the more deactivations the species would experience, which in turn leads to higher maximum

RE (third trend). This is the reason why the pressure based approach is sensitive to the length of the well.

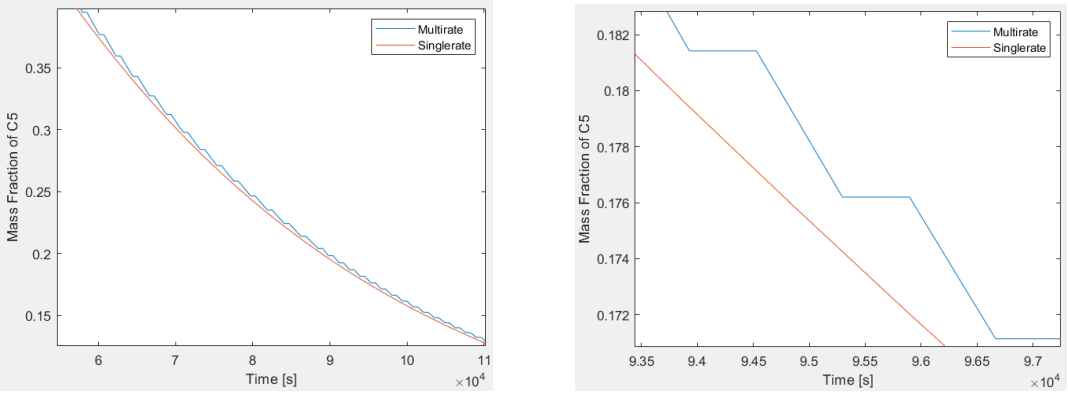

Figure 6.21: Left: Mass fraction of pentane using multirate and single-rate approaches. Right: Zoomed-in illustration of the figure to the left. The permeability and the length of the well used here are $\kappa = 10^{-13}\,\mathrm{m}^2$ and 50 m, respectively.

Looking to the right of Fig. 6.19, it is obvious that the well subsystem is deactivated much more rapidly in the first 10^5s than in the following period. This is due to the gradient of the pressure at the interface being large in that period before stabilizing at around $\frac{\partial p}{\partial t} = 1\,\mathrm{Pa/s}$. A high pressure gradient means that the activation criterion of Δp is met rapidly, which in turn leads to the activation of the well subsystem. Using automatic activation and deactivation based only on pressure leads to results that not always show a consistent propagation of maximum RE as shown in Fig. 6.20. The reason behind this is that when the well subsystem is activated, the pressure in the fluid inside the well is propagated with the speed of sound as mentioned earlier, hence the deactivation criterion $\frac{\partial p}{\partial t} = 10\,\mathrm{Pa/s}$ is reached in a short time. At the same time, the species in the well are transported with the fluid velocity u. In other words, the activation and deactivation processes occur independent of the content in the well. Thus, measuring the content of an unflushed well in relation to the activation and deactivation processes does not yield fully correlated results.

Chapter 7

Discussion

In this study, the relative error of using multirate approach in comparison with single-rate approach was measured in each simulation case. The time steps in the well subsystem outside the dynamic region was observed to be around 15 s in most of the simulations (less than 15 s in the dynamics region), while in the reservoir subsystem on the other hand, the time step was chosen to be 300 s (when the well subsystem is deactivated). This yields a time step ratio of at least 20 between the two subsystems throughout the simulation. In other words, deactivating the well subsystem enables the system to move from a time step of 15 s to 300 s. How much time was saved in total compared to the error induced by the deactivation is the matter of discussion in this chapter.

7.1 Time Consumption Vs. Error

The time it takes to simulate one of the cases (simulation time) presented in this study differs from a computer to another depending on factors such as processor power, RAM and memory size. However, running the simulations one at a time with the same computer can provide a basis for comparing the simulation time of each case. The results in Fig. 7.1 show the time it took to simulate some of the cases in this study using both time and pressure based deactivation.

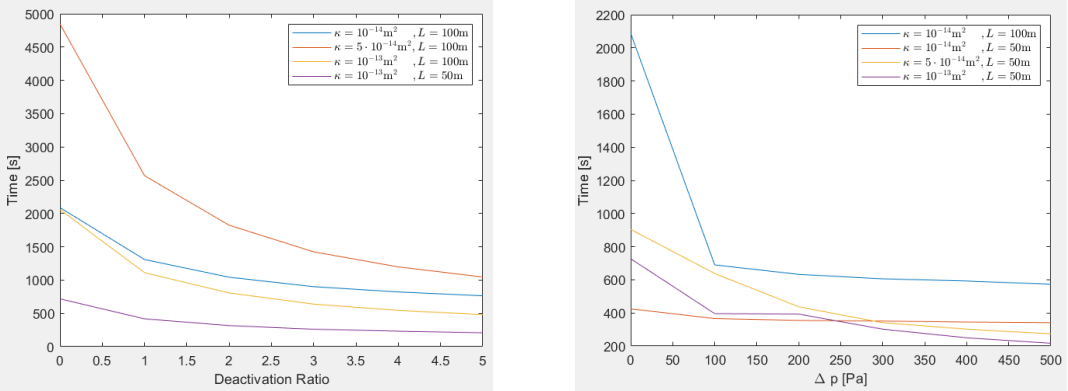

Figure 7.1: Left: Simulation time using time based deactivation. Right: Simulation time using pressure based deactivation

Fig. 7.1 shows that the simulation time decreases with the deactivation ratio and Δp, which is to be expected. When it comes to the time based deactivation, the simulation time is proportional with L and inversely proportional with κ except for the case with $\kappa = 5 \cdot 10^{-14}\,\mathrm{m}^2$. The reason for this is that having a shorter L leads to fewer amount of control volumes that need to be calculated at each time step. In addition, by increasing κ, the flow in the reservoir becomes faster, hence, the time it takes for the reservoir to reach the same condition using a lower κ is less. This is due to the time step in the reservoir subsystem being constant (300 s) and independent of permeability. In the case with $\kappa = 5 \cdot 10^{-14}\,\mathrm{m}^2$, the software uses longer time to converge at each time step, hence the deviation in simulation time compared to the other cases. On the other hand, using pressure based deactivation yields the same simulation time trend when it comes to L as in the case of time based deactivation. However, the trend is not clear for different values of κ.

Looking to the left of Fig. 7.1, it can be seen that the curves become more flat after a deactivation ratio of 2, which means that the saving in simulation time becomes less significant. According to Fig. 6.12, the maximum RE increases linearly with the deactivation ratio. Hence, the most efficient deactivation ratio is 2. In the case of using $\kappa = 5 \cdot 10^{-14}\,\mathrm{m}^2$ and $L = 100\,\mathrm{m}$, the simulation time using single-rate approach is 4847 s, while using a deactivation ratio of 2, the simulation time becomes 1824 s. In other words, accepting a maximum RE of 1.4% (see Fig. 7.1), the simulation time can be reduced by 63% in this particular case.

On the other hand, the right hand side of Fig. 7.1 shows that the curves become more flat after $\Delta p = 100\,\mathrm{Pa}$, while the maximum RE keeps increasing with Δp according to Fig. 6.20. Therefore, using $\Delta p = 100\,\mathrm{Pa}$ is the most efficient criterion for activating the

well subsystem when using pressure based deactivation. In the case of using $\kappa = 10^{-14}\,\mathrm{m}^2$ and $L = 100\,\mathrm{m}$, the simulation time using single-rate approach is 2088 s, while using an activation criterion of $\Delta p = 100\,\mathrm{Pa}$, the simulation time becomes 690 s. In other words, accepting a maximum RE of 0.6% (see Table 6.3), the simulation time can be reduced by 67% in this particular case.

After having analyzed the time-saving aspects of both deactivation approaches, there is now sufficient data to investigate the maximum RE and simulation time in comparison with deactivation ratio and Δp. Fig. 7.2 illustrates two cases of such comparison where each case is tested with both deactivation approaches, which are referred to as "Time" and "Pressure". Both deactivation ratio and Δp are represented in the horizontal axis in Fig. 7.2. In case of using the horizontal axis to represent the increments of Δp, the values must be multiplied by 100 to obtain the correct scale.

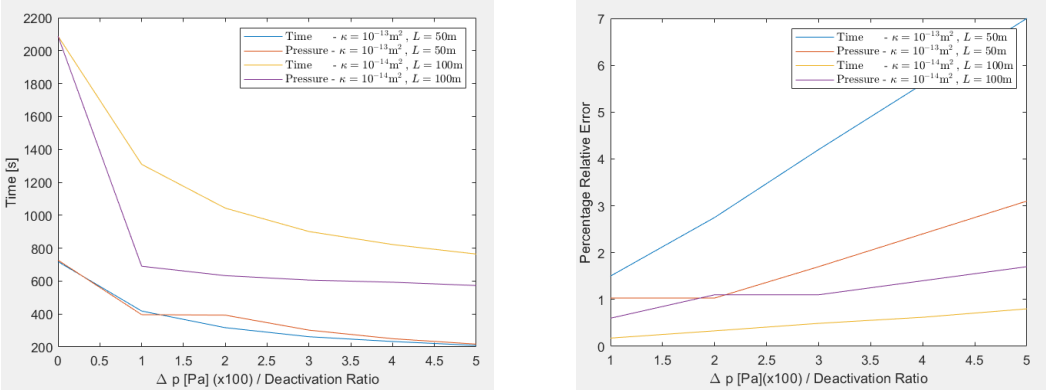

Figure 7.2: Left: Relationship between simulation time and deactivation ratio/Δp. Right: Relationship between maximum RE and deactivation ratio/Δp.

In the case of pressure based deactivation where $\kappa = 10^{-14}\,\mathrm{m}^2$ and $L = 100\,\mathrm{m}$ are used, see Fig. 7.2, the simulation time is lower while the maximum RE is higher than the case using time based deactivation. This is true for all values along the horisontal axis. The reason behind this trend is that the permeability is relatively low, hence the pressure change in the reservoir is slow. As a result, the well subsystem remains deactivated for long periods of time when using pressure based deactivation. Thus, the error becomes higher and the simulation time lower than in the case when the well subsystem is manually controlled using time based deactivation.

Furthermore, In the case where $\kappa = 10^{-13}\,\mathrm{m}^2$ and $L = 50\,\mathrm{m}$ are used, see Fig. 7.2, the error is always lower using deactivation based on pressure rather than time, while the simulation time is almost the same except for when $\Delta p = 200\,\mathrm{Pa}$. The reason behind this trend is that the permeability is relatively high here, hence the pressure change in the

reservoir is fast. As a result, the well subsystem is activated and deactivated rapidly in the dynamic region, thus, the error is always lower using deactivation based on pressure rather than time (due to high pressure gradient). However, outside the dynamic region where the pressure gradient is low, the well remains deactivated for long periods of time when deactivation based on pressure is used. In other words, using pressure based deactivation leads to higher simulation time in the dynamics region but lower outside the dynamic region in comparison to the time based deactivation. This leads to an average simulation time that is almost similar to the case when time based deactivation is used. Last, it is worth mentioning that there is no standard for how large maximum RE is acceptable. Such criterion is unique to each case based on the physics involved and the willingness of the user to reduce the simulation time.

7.2 Further Work

The results from Fig. 7.2 show that if the permeability is high, then pressure deactivation is preferred due to its advantage over the time based deactivation when it comes to maximum RE (both yield almost the same simulation time). However, caution must be exercised in the latter case as the pressure based deactivation is sensitive to the length of the well. In other words, using large L might lead to maximum RE higher than in the case of using time based deactivation even if the permeability is low. Therefore, more tests must be conducted to map the full effect of well length in regard to maximum RE using pressure based deactivation.

7.2.1 Hybrid Approach

The advantage of using time based deactivation is that it ensures the content of the well is flushed out at least once such that the condition in the well is updated in regard to the reservoir. The disadvantage of the approach is that it does not take into the consideration the dynamics of the reservoir. On the other hand, the advantage of using pressure based deactivation is that it takes into consideration the dynamics of the reservoir, while the downside of the approach is that it does not guarantee that the content of the well is updated with the reservoir. In other words, each deactivation approach has its advantages and disadvantages. However, it is possible to merge the best of the two worlds into a new hybrid approach that might be far more superior than each of the two deactivation approaches. To accomplish this, the well subsystem must be active for a predefined period of time to ensure the well is updated with the reservoir before being deactivated. On the

other hand, the activation criterion must be based on Δp at the interface between the well and the reservoir to take into the consideration the dynamics of the reservoir. As a result, the hybrid approach would be able to both update the content of the well and adapt to the dynamics of the system at the same time.

The pressure based deactivation was used in this study due to its correlation with the fluid velocity in a reservoir, which in turn is the variable that determines how fast mass is transported in a reservoir. However, the approach does not take into consideration the changes in mass fraction directly (ΔC) or the changes in temperature ($\Delta\Theta$). The latter can be important in cases where there are large temperature variations in the reservoir (phase changes might occur). Therefore, the hybrid approach can be constructed such that it adds more activation constraints such as $\Delta\Theta$ and ΔC in addition to Δp. Adding these constraints would make the hybrid approach even more robust and adaptive to different reservoir conditions, which in turn would lead to results closer to the case using single-rate approach.

7.2.2 Slow-First Approach With a Jump

Both time and pressure based deactivation approaches entail having the same time step for both subsystems when the well subsystem is activated, which in best case can be 15 s as mentioned earlier (outside the dynamic region). Using such a small time step in the reservoir subsystem is a waste of computational power considering that the reservoir subsystem is slow changing. To avoid this, a new approach based on the slow-first approach (Subsection 2.3.1) is recommended, see Fig. 7.3 for illustration.

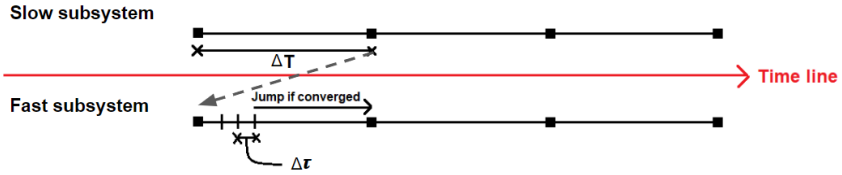

Figure 7.3: Sketch of a slow-first approach with a jump. The fast and the slow subsystem refer to the well and the reservoir, respectively. The time step ΔT is used in the slow subsystem, while the time step $\Delta\tau$ is used in the fast subsystem.

The suggestion is to calculate the variables in the reservoir subsystem first using the most suitable time step for it (300 s was chosen in this study). Second, the new values from the reservoir subsystem are used as a boundary condition to update the conditions in

the well subsystem. The time step in the well subsystem can either be constant, or it can be automatically adjusted based on its respective stability criteria (based on a self-adjusting method). Last, the idea is that the well subsystem is simulated in time until a certain convergence criterion is met. In that case, the well subsystem is said to be updated and the clock in the subsystem is then jumped to match the one at the boundary condition, i.e. the reservoir subsystem, as shown in Fig. 7.3. The reason behind the jump is to avoid wasting computational power when there is little change in the well subsystem.

The convergence criterion can, for instance, be based on measuring the difference in mass fraction of a component k in the Measurement CV between two subsequent time steps (n and $n+1$), see Eq.(7.1). If the value of "Test" from Eq.(7.1) is under a predefined value (tolerance), the well subsystem can be said to be converged. The convergence criterion can also be based on several parameters such as temperature and pressure to ensure overall accuracy. In other words, the well subsystem is said to be updated when all the convergence criteria are met.

$$Test = \sqrt{(Y_k^{n+1} - Y_k^n)^2} \tag{7.1}$$

Chapter 8

Conclusions

8.1 Conclusions

This thesis investigated the possibilities of reducing reservoir simulation time while maintaining acceptable accuracy. The rate of change in the conditions both in the reservoir and well subsystems were investigated and utilized. The main conclusions from the work are presented in this chapter.

In Chapter 6, two approaches were used to activate and deactivate the well subsystem based on time and pressure. The mass fraction of pentane obtained using these two approaches were compared against the results from using single-rate approach, where the well subsystem remained active throughout the simulation time. The maximum relative error (maximum RE) was used as basis for comparison between all the cases that were simulated. The permeability of the reservoir and the well length are the only two physical variables that where varied in addition to deactivation ratio and Δp.

The time based deactivation approach has shown to be predictable as the maximum RE is linearly proportional with both deactivation ratio and permeability. The latter is a direct consequence of using Darcy's law which states that permeability is linearly proportional with fluid velocity in reservoir, when all the other variables are kept constant (μ and ∇p). The approach has also shown not be sensitive to well length since the well subsystem remains active for a predefined period of time. This is to ensure that the content in the well is updated with the reservoir, which is the main advantage of using this approach. Hence, the longer the well, the longer the activation period must be. The disadvantage of using this approach is that it does not take into consideration the dynamics of the system, i.e. regions with high gradients, as the deactivation period is also predefined by the user.

The pressure based deactivation approach has shown not be as predictable as the time based deactivation. However, the trends that have been observed using pressure based deactivation can help anticipating the behaviour of this approach. The first and the most obvious trend is that the maximum RE increases with Δp. The second is that the maximum RE , as in the case when using time based deactivation, is proportional with permeability. On the contrary to the time based deactivation, the proportionality is not linear. The third trend is that this approach is sensitive to well length. The reason for this is that the well subsystem is deactivated based on pressure gradient in the well regardless of whether or not the content of the well is updated with the reservoir, which is obviously the main disadvantage of this approach. Hence, the longer the well length, the more deactivation a particle in the well subsystem would experience, which in turn leads to a higher maximum RE. The advantage of this approach, however, is that it takes into consideration the dynamics of the system.

The results from Section 7.1 have shown that the time based deactivation approach yields the less maximum relative error when the permeability is low. On the other hand, if the permeability of the reservoir is high, then the pressure based deactivation is preferred. The reason for this, in a nutshell, is that when the permeability is high, the reservoir subsystem becomes fast changing. Hence the approach that adapts the most to a dynamical system must be chosen, which is deactivation based on pressure. Furthermore, the advantage of using deactivation approach based on pressure rather than time is that it is automatic. In other words, the user of the software does not need to analyse the distribution of the hydrocarbons in the reservoir in order to choose the most suitable activation and deactivation criteria.

Moreover, the most efficient deactivation ratio and Δp was found to be 2 and 100 Pa, respectively. The results have shown that by deactivating the well subsystem, i.e. using multirate approach, the reservoir subsystem is altered permanently due to the two subsystems being strongly coupled. Hence, using multirate approach in regard to reservoir simulation always introduces additional errors.

Bibliography

[1] Zhen Liu. *Multiphysics in Porous Materials*. Springer, 2018.

[2] David Kan. What is multiphysics? https://www.comsol.com/blogs/what-is-multiphysics/. Accessed: 2019-05-27.

[3] Arun Tangirala, Rohit Patwardhan, Sirish Shah, and Tongwen Chen. Performance comparison of multirate vs. single-rate systems. *IFAC Proceedings Volumes*, 33(10):443 – 448, 2000. IFAC Symposium on Advanced Control of Chemical Processes 2000, Pisa, Italy, 14-16 June 2000.

[4] Emil Constantinescu and Adrian Sandu. Multirate timestepping methods for hyperbolic conservation laws. 33(3):239–278, 2007.

[5] Valeriu Savcenco. Construction of a multirate rodas method for stiff odes. *Journal of Computational and Applied Mathematics*, 225(2):323 – 337, 2009.

[6] Mariesa Crow and Jingguang Chen. The multirate simulation of facts devices in power system dynamics. In *Proceedings of Power Industry Computer Applications Conference*, pages 290–296. IEEE, 1995.

[7] Saber Samee. *Multi-physic simulation of physical processes with different time-constants*. Pre-master's project, Norwegian University of Science and Technology, 2018.

[8] Toshiji Kato, Kaoru Inoue, Takayuki Fukutani, and Yoshinori Kanda. Multirate analysis method for a power electronic system by circuit partitioning. *IEEE Transactions on Power Electronics*, 24(12):2791–2802, 2009.

[9] Farshid Nazari and Ramachandran Nair. A Godunov-type finite-volume solver for nonhydrostatic euler equations with a time-splitting approach. *Journal of Advances in Modeling Earth Systems*, 9(1):465–481, 2017.

[10] Implications of surface wave data measurement uncertainty on seismic ground response analysis. *Soil Dynamics and Earthquake Engineering*, 61-62:239 – 245, 2014.

[11] Christian Kuehn. *Multiple Time Scale Dynamics*, volume 191. Springer, 2015.

[12] Bernd Markert. *Weak or Strong : On Coupled Problems in Continuum Mechanics; Schwach oder Stark : über gekoppelte Probleme der Kontinuumsmechanik*. Universität Stuttgart, 2010.

[13] Woinshet Mergia and Kailash Patidar. Fractional-step -method for solving singularly perturbed problem in ecology. *Advances in Computational Mathematics*, 44(3):645–671, 2018.

[14] David Keyes, Lois McInnes, Katherine Evans, and Judith Hill. Multiphysics simulations: Challenges and opportunities. *International Journal of High Performance Computing Applications*, 27(1), 2013.

[15] Felix Mihai, Inja Youn, and Padmanabhan Seshaiyer. Multiphysics modeling and simulation of fluid-structure interaction applied to biological problems. *Procedia Computer Science*, 9:615 – 623, 2012. Proceedings of the International Conference on Computational Science, ICCS 2012.

[16] Carlos Felippa, Kwang Park, and Charbel Farhat. Partitioned analysis of coupled mechanical systems. *Computer Methods in Applied Mechanics and Engineering*, 190(24):3247 – 3270, 2001. Advances in Computational Methods for Fluid-Structure Interaction.

[17] Kwang Park and Carlos Felippa. A variational framework for solution method developments in structural mechanics. *Journal of Applied Mechanics*, 65(1):242–249, 1998.

[18] Zhiqiang Zhai. *Developing an integrated building design tool by coupling building energy simulation and computational fluid dynamics programs*. PhD thesis, Massachusetts Institute of Technology, 2003.

[19] S. R. Novascone, B. W. Spencer, D. Andrs, R. L. Williamson, J. D. Hales, and D. M. Perez. Results from tight and loose coupled multiphysics in nuclear fuels performance simulations using bison. *Mathematics Computation,Sun Valley Idaho*, 2013.

[20] Makoto Yamamoto. Multi-physics cfd simulations in engineering. *Journal of Thermal Science*, 22(4):287–293, 2013.

[21] Kai Schneider, Dmitry Kolomenskiy, and Erwan Deriaz. Is the cfl condition sufficient? some remarks. In *The Courant–Friedrichs–Lewy (CFL) Condition*, pages 139–146. Springer, 2013.

[22] Ekaterina Brocke, Upinder S Bhalla, Mikael Djurfeldt, Jeanette Hellgren Kotaleski, and Michael Hanke. Efficient integration of coupled electrical-chemical systems in multiscale neuronal simulations. *Frontiers in Computational Neuroscience*, 10:97, 2016.

[23] Marija Trcka. *Co-simulation for Performance Prediction of Innovative Integrated Mechanical Energy Systems in Buildings*. Technische Universiteit Eindhoven, 2008.

[24] Ekaterina Brocke, Mikael Djurfeldt, Upinder Bhalla, Jeanette Kotaleski, and Michael Hanke. Multirate method for co-simulation of electrical-chemical systems in multiscale modeling. *Journal of Computational Neuroscience*, 42(3):245–256, 2017.

[25] Johnny Chang, Scott Ploen, Garett Sohl, and Bryan Martin. Parallel multistep/multi-rate integration of two-time scale dynamic systems. In *AIAA Modeling and Simulation Technologies Conference and Exhibit*, page 5162, 2004.

[26] Frank Harris. Chapter 13 - Integral Transforms. In Frank E. Harris, editor, *Mathematics for Physical Science and Engineering*, pages 453 – 486. Academic Press, Boston, 2014.

[27] Wim van Drongelen. Chapter 6 - Continuous, Discrete, and Fast Fourier Transform. In Wim Drongelen, editor, *Signal Processing for Neuroscientists (Second Edition)*, pages 103 – 118. Academic Press, second edition edition, 2018.

[28] Ali Bekir Yildiz. Determination of unified time constants of switching circuits in terms of averaged-nodal equations. *Automatika*, 58(1):11–17, 2017.

[29] Woinshet Mergia and Kailash Patidar. Efficient simulation of a slow-fast dynamical system using multirate finite difference schemes. *Quaestiones Mathematicae*, 39(5):689–714, 2016.

[30] Luca Bonaventura, Francesco Casella, Ludovica Delpopolo, and Akshay Ranade. A self adjusting multirate algorithm based on the tr-bdf2 method. *arXiv preprint arXiv:1801.09118*, 2018.

[31] OpenCFD. 6.1 Time and data input/output control. https://www.openfoam.com/documentation/user-guide/controlDict.phpx22-830006.1. Accessed: 2019-05-29.

[32] Da Silva and Jan Jansen. A review of coupled dynamic well-reservoir simulation. *IFAC-PapersOnLine*, 48(6):236–241, 2015.

[33] Malay Das, Partha Mukherjee, and Kambadur Muralidhar. Equations governing flow and transport in porous media. In *Modeling Transport Phenomena in Porous Media with Applications*, pages 15–63. Springer, 2018.

[34] Abdon Atangana. Chapter 2 - Principle of Groundwater Flow. In Abdon Atangana, editor, *Fractional Operators with Constant and Variable Order with Application to Geo-Hydrology*, pages 15 – 47. Academic Press, 2018.

[35] Olusegun Olalekan Alabi. Validity of darcy's law in laminar regime. *The Electronic Journal of Geotechnical Engineering*, 16:27–40, 2011.

[36] Glenn Brown. Darcy's law basics and more. https://bae.okstate.edu/faculty-sites/Darcy/LaLoi/Basics.htm. Accessed: 2019-05-30.

[37] Donald Nield. Modelling fluid flow and heat transfer in a saturated porous medium. *Advances in Decision Sciences*, 4(2):165–173, 2000.

[38] Matthis Thorade and Ali Saadat. Partial derivatives of thermodynamic state properties for dynamic simulation. *Environmental Earth Sciences*, 70(8):3497–3503, 2013.

[39] Evgeny Chekhonin, Anton Parshin, Dimitri Pissarenko, Yury Popov, Raisa Romushkevich, Sergey Safonov, Mikhail Spasennykh, M Chertenkov, and V Stenin. When rocks get hot: thermal properties of reservoir rocks. *Oilfield Review*, 24(3):20–37, 2012.

[40] Petroleum engineering handbook : Volume v, : Reservoir engineering and petrophysics, 2007.

[41] Alfredo Leon-G, Luis Sanchez, B Jose, C Fernando Ascencio, G Juan E Ladron, Agustin Galindo, Fernando Samaniego-V, Heber Cinco Ley, Fernando Rodriguez, et al. A study of the initial and exploitation conditions of the super giant akal offshore naturally fractured reservoir. In *18th World Petroleum Congress*. World Petroleum Congress, 2005.

[42] Fekete Associates Inc. Reservoir flow. https://bit.ly/2WuJglI. Accessed: 2019-05-30.

[43] Tarek Ahmed. Chapter 1 - Fundamentals of Reservoir Fluid Behavior. In Tarek Ahmed, editor, *Reservoir Engineering Handbook (Fourth Edition)*, pages 1 – 28. Gulf Professional Publishing, Boston, fourth edition edition, 2010.

[44] James Sheng and Ke Chen. Evaluation of the EOR potential of gas and water injection in shale oil reservoirs. *Journal of Unconventional Oil and Gas Resources*, 5:1–9, 2014.

[45] José Vazquez Taboada. Design for operation and maintenance of the Johan Sverdrup oil and gas field. 2014.

[46] Sedat Biringen. A note on the numerical stability of the convection-diffusion equation. *Journal of Computational and Applied Mathematics*, 7(1):17–20, 1981.

[47] Jérémie Messud, Mathieu Reinier, Hervé Prigent, Patrice Guillaume, Thierry Coléou, and Sylvain Masclet. Extracting seismic uncertainties from tomographic velocity inversion and their use in reservoir risk analysis. *The Leading Edge*, 36(2):127–132, 2017.

[48] Boyun Guo, Xinghui Liu, and Xuehao Tan. Chapter 7 - Forecast of Well Production. In Xinghui Liu Boyun Guo and Xuehao Tan, editors, *Petroleum Production Engineering (Second Edition)*, pages 179 – 196. Gulf Professional Publishing, Boston, second edition edition, 2017.

[49] Dan Vladimir Nichita, Daniel Broseta, and Claude Leibovici. Reservoir fluid applications of a pseudo-component delumping new analytical procedure. *Journal of Petroleum Science and Engineering*, 59(1-2):59–72, 2007.

[50] Tamás Insperger and Gábor Stépán. Semi-discretization method for delayed systems. *International Journal for Numerical Methods in Engineering*, 55(5):503–518, 2002.

[51] Jisheng Kou, Shuyu Sun, and Bo Yu. Multiscale time-splitting strategy for multiscale multiphysics processes of two-phase flow in fractured media. *Journal of Applied Mathematics*, 2011, 2011.

[52] Juan Sebastian Lopez-Echeverry, Simon Reif-Acherman, and Eduard Araujo-Lopez. Peng-robinson equation of state: 40 years through cubics. *Fluid Phase Equilibria*, 447:39 – 71, 2017.

[53] Henk Kaarle Versteeg and Weeratunge Malalasekera. *An Introduction to Computational Fluid Dynamics: The Finite Volume Method*. Pearson education, 2007.

[54] Kayode Coker. *Fortran programs for chemical process design, analysis, and simulation*. Elsevier, 1995.

[55] Don Andrew Duggan-Haas, Robert Ross, and Warren Allmon. *The Science Beneath the Surface: A Very Short Guide to the Marcellus Shale*. Paleontological Research Institution, 2013.

[56] Knut Bjørlykke. *Petroleum Geoscience: From Sedimentary Environments to Rock Physics*. Springer Science & Business Media, 2010.

[57] Harsh Gupta and Sukanta Roy. Chapter 2 - Basic Concepts. In Harsh Gupta and Sukanta Roy, editors, *Geothermal Energy*, pages 15 – 30. Elsevier, Amsterdam, 2007.

[58] RE Folinsbee. The future supply of nature-made petroleum and gas: Technical report. *Geoscience Canada*, 5(3), 1978.

[59] Saifaddeen Sallam, Mohammad Munir Ahmad, and Mohamed Nasr. The effect of water injection on oil well productivity, 2015.

[60] Jincheng Mao, Jiawei Liu, Haibin Wang, Xiaojiang Yang, Zhaoyang Zhang, Bo Yang, and Jinzhou Zhao. Novel terpolymers as viscosity reducing agent for tahe super heavy oil. *RSC Advances*, 7(31):19257–19261, 2017.

[61] Willem Hundsdorfer, Anna Mozartova, and Valeriu Savcenco. Analysis of explicit multirate and partitioned runge-kutta schemes for conservation laws. 2007.

[62] Gustavo Rodríguez-Gómez, Pedro González-Casanova, and Jorge Martínez-Carballido. Computing general companion matrices and stability regions of multirate methods. *International Journal for Numerical Methods in Engineering*, 61(2):255–273, 2004.

[63] Harald Soleng and Lars Holden. Gridding for petroleum reservoir simulation. *Numerical Grid Generation in Computational Field Simulations, edited by Cross, M., Soni, BK, Thompson, JF, Hauser, J. and Eiseman, PR, Missisipi State University*, 1998.

Appendix A

Oil and Gas

A.1 Origin of Oil and Gas

The major energy source in the world, and one that has powered our civilization in the past decades, was actually formed and stored many hundred million years ago. In the ancient geological ages, such as the Devonian age which lasted from 419 to 359 million years ago, microscopic animals and plants that lived in the ocean stored the energy from the sun as carbon molecules[55]. As these animals and plants died and sunk to the bottom of the ocean, more and more layers of sediments were formed throughout millions of years. Eventually, the amount of heat and pressure in addition to type of the biomass determined if the relic of the animal and plant became oil or gas.

A.2 Seismic Survey

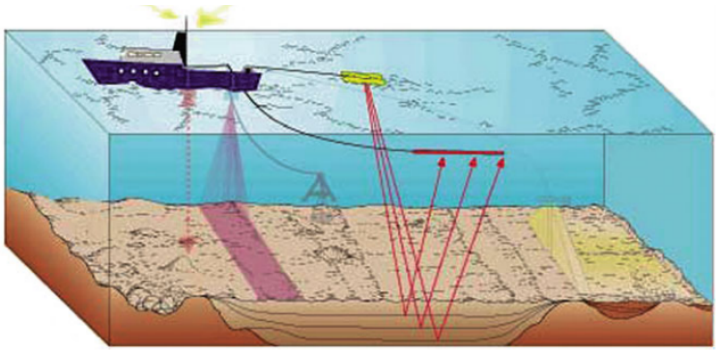

Figure A.1: Sound waves generated from the transducers are captured back by the receivers[56].

The first step in oil and gas exploration starts from seismic surveys that consist of a specialized boat, in case of offshore surveying, which tows two essential equipments, the

transducers and the receivers as shown in Fig. A.1. The transducers send pulses of ultra sound waves from different positions which are then captured by the receivers. The receivers are located in a specific distance away from the transducers. The raw data acquired by the receivers is then processed using techniques in signal processing to obtain a 2D or 3D images of the reservoir as shown in Fig. A.2[56]. The time it takes for the sound waves to reach the receivers in addition to some other wave properties determine the composition, type of fluids and the porosity at different depths[56]. Such data are then used as basis for reservoir simulations as in Chapter 6. It is worth mentioning that the deeper the layers are, the more uncertain the seismic data become[47].

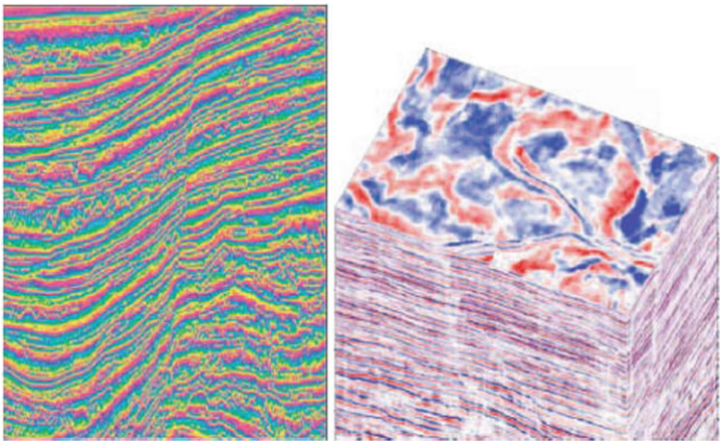

Figure A.2: 2D (left) and 3D (right) illustration of a typical seismic data[56].

After having located the regions containing oil and gas in a reservoir, the next step is to drill a well to extract the hydrocarbons. Wells are used for different purposes such as production, where oil and gas is pumped through, or injection, where an injection fluid is used to enhance the production in the field (see Appendix A.4). Fig. A.3 illustrates two well configurations, a horizontal and a vertical one.

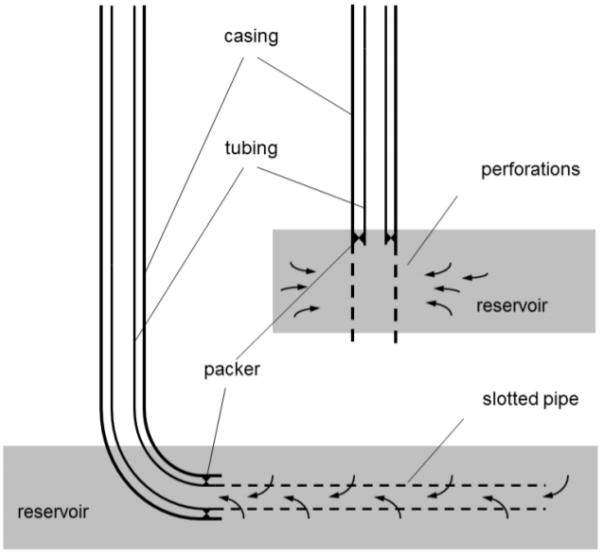

Figure A.3: The lower and the upper reservoirs in the figure are drained using horizontal and vertical well, respectively[32]. The terms casing, tubing, perforations and slotted pipe are not of interest here.

A.3 Reservoir Thermal Properties

Most of the oil and gas reserves that are of economical interest are found in the crust of the earth[57], which is the outermost layer of the earth. The crust beneath the oceans tend to be thinner than the continental ones resulting in an average thickness of 35 km[57]. Fig. A.4 shows the different layers of the earth.

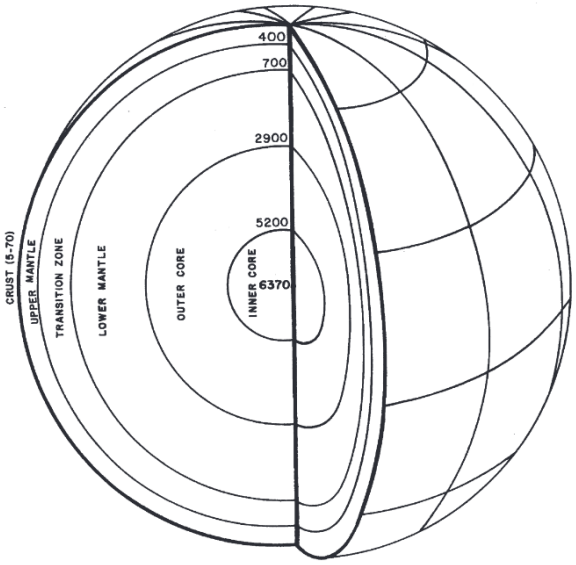

Figure A.4: Cross section of the earth[57].

In naturally fractured reservoirs, where the effective permeability is high, the convective

velocity induced by geothermal temperature gradients becomes significant. This leads to the flow of warmer and lighter fluids upwards displacing colder and more dense fluids, which moves downwards. As a result, the temperature in the reservoir becomes more smeared and the geothermal gradients become small[41]. Changes in temperature can also have a direct effect on the thermal properties of a reservoir such as thermal conductivity and diffusivity. For instance, a study conducted on samples from the Yarega oil field in Russia showed that under an increase of temperature from 25°C to 100°C, the thermal conductivity and diffusivity decreased by 50% and 70%, respectively[39]. Furthermore, Fig. A.5 shows that the thermal conductivity, diffusivity and volumetric heat capacity of different types of rocks seem to oscillate around an equilibirium value along ground depth.

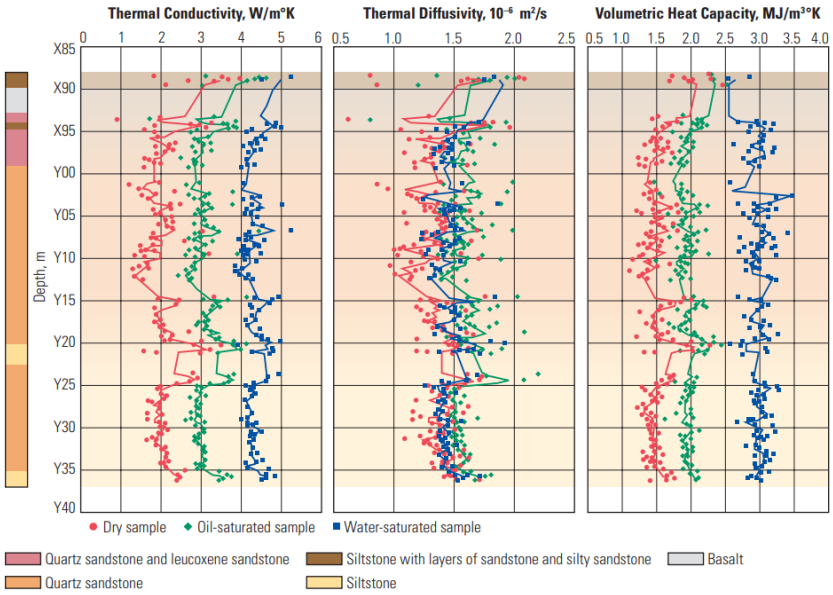

Figure A.5: Thermal properties of different types of rocks[39].

It is also worth mentioning that when simulating the heat exchange between a well and the reservoir around, the effect of different heat capacity in the rock formations in the reservoir must also be accounted for. This is due to different heat capacities giving rise to different temperature profiles in a reservoir, which in turn would affect the temperature in the well.

A.4 Production Enhancement by Injection

The initial flow into a well is driven by the natural pressure in a reservoir, given the pressure is above a certain threshold to sustain an economical production rate. When the pressure is beneath the threshold, a secondary recovery method is needed in order to

increase the pressure again. Such recovery methods include injecting of a miscible gas, water or steam through an injection well([44],[58],[59]). The idea of injecting gas is to both increase the pressure in the reservoir, and at the same time, decrease the viscosity of the oil upon mixing[44]. The reduction of the viscosity would increase the effective permeability, which is proportional to the fluid velocity according to Darcy's law, and as a result, more oil can be recovered. The same principle is applied when injecting hot steam into a reservoir. The heat introduced into the reservoir via the steam injection leads to decrease in the viscosity of the oil as shows in Fig. A.6[58].

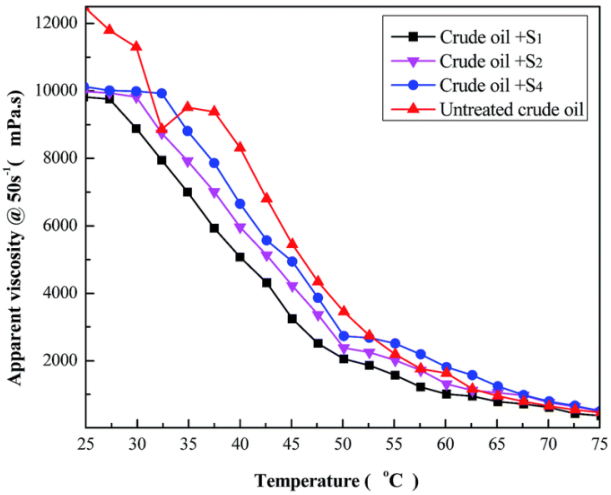

Figure A.6: Viscosity vs. temperature of different types of heavy hydrocarbons[60]. It is the trend that is of concern here and not the specific type of the hydrocarbons.

Unlike gas and steam injection, water injection does not reduce the density of the hydrocarbons in the reservoir since they are two immiscible fluids due to their polarity and difference in density. It is however the difference in density that is exploited in this case. Since water is more dense than hydrocarbons in both liquid and gaseous phase, by injecting water into a reservoir, hydrocarbons are pushed away towards the production well as a result of increase in pressure[59]. Increasing the pressure in a reservoir leads to higher pressure gradients between the reservoir and the well. Again, according to Darcy's law, an increase in the pressure gradient is proportional to an increase in the flow rate. Furthermore, a study has shown that gas injection is more suitable recovery method than water injection when the permeability of the matrix is ultra low[44].

Appendix B

Numerical Stability of Multirate Approach

Both spatial and time components of a PDE system need to be discretized in a manner such that the overall stability and accuracy of the simulation is preserved. When it comes to time discretization, both implicit and explicit methods can be used. However, the latter method tends to be very expensive when solving for stiff PDEs with advection part due to severe restrictions on the time step size. In order to overcome the issue of using small time step, implicit methods can be used instead which are unconditionally stable[61] within the same subsystem. The downside of using implicit methods is that the solution of a nonlinear system is needed at each time step, which in turn may lead to an increase in computational cost. Explicit methods are often preferred in cases where the overall system is not large and small time step is needed for accuracy, such as in explosion simulations. However, using explicit multirate schemes for conservation laws can either be locally inconsistent and mass conservative, or consistent but not mass conservative[61].

Furtheremore, and as mentioned earlier, each subsystem is normally discretized such that the stability criteria is met within the subsystem. This, however, does not ensure that the entire system is stable upon coupling the subsystems in a multiphysics problem. For instance, using implicit Euler method to a stable oscillating subsystem may lead to the amplification of the oscillatory behaviour upon coupling to other subsystems. This may occur due to inherent properties in the components such as stiffness[22]. Since each multiphysics problem can be solved using different multirate approaches (i.e. using different types of coupling strategies and multirate philosophies), the stability for each system must be analysed independently. In other words, the complexity of mulirate systems avert any attempts to obtain a generalized theory on stability. According to Gomez et al. "One of the major problems concerning the use of multirate methods to solve real life problems

is the lack of general theoretical results that guarantee their absolute stability[62]." The trend is, however, that the strength of coupling between subsystems or the stiffness of the system is inverse proportional with the stability region of multirate approaches[30]. Analysis on the stability of multirate approaches using a trapezoidal and semi-implicit linear discretization method, for instance, are presented in [6] and [62], respectively.

Appendix C

Upscaling of Grid in Reservoir Simulation

The reservoir type that is of concern in this study is assumed to be homogeneous and isotropic. Homogeneous means that the scalar properties in the reservoir are the same everywhere, such as porosity. On the other hand, an isotropic reservoir means that the vector properties are the same in all directions, hence permeability is expressed by the constant κ. This part discusses the problems that can occur in regard to setting up a numerical grid in the reservoir. The content is taken from Soleng and Holden[63] and is presented as general information and not necessarily coupled to the simulations in this study.

The process of generating a grid in a reservoir starts from the geological data obtained by the seismic survey as discussed in Appendix A.2. The output data of such models is then generated on a fine scale in order to capture as much details as possible of the heterogeneities within the field. Data from a fine scale model is beneficial when predicting the fluid flow in the system accurately. However, a much coarser grid is desirable in order to reduce the computational cost. A way to do so is to scale up the permeability data to a coarser representation by averaging data in the cells nearby. The averaging approach, although being a normal procedure in many other applications, can be problematic in this case as permeability is a non-additive property.

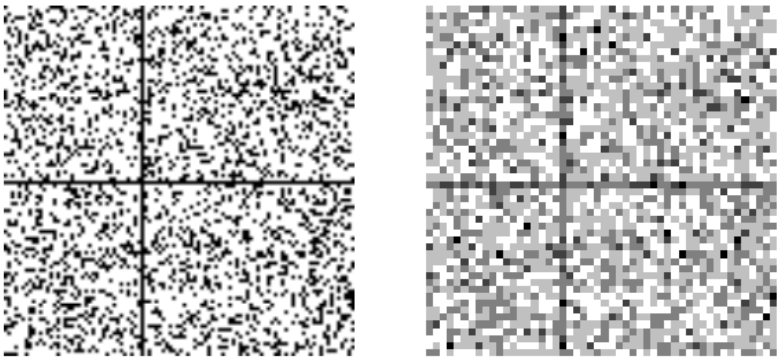

Figure C.1: Illustration of fine grid to the left and coarse grid to the right[63].

Averaging the permeability of porous media with abrupt changes in heterogeneity can have significant consequences as depicted in Fig. C.1. The part to the left in the figure shows porous media divided into four regions with impermeable walls in between. By averaging the entire domain and moving to a coarser grid, such as the one shown to the right of the figure, the impermeable walls now become layers with low permeability instead. Fluid flow can now seep between all the four regions, which is unphysical in reality. The challenge lies in upscaling without loosing much in precision, or at least, not leading to an unrealistic condition. Caution must therefore be exercised when upscaling in regions where the gradient of heterogeneity is high. A solution to this problem can be, for instance, using a hybrid grid system where fine scale is used in regions with high heterogeneity, while a more coarse scale used in the rest of the domain. Needles to say, in the case of having homogeneous reservoir, the averaging approach can be a very efficient tool since the error in upscaling becomes negligible.